STATISTICS, OPTIMIZATION AND INFORMATION COMPUTING
Stat., Optim. Inf. Comput., Vol. **16**, December 2026, pp 6435–6475.
Published online in International Academic Press (www.IAPress.org)

A New Topp-Leone Modified Kies-G Power Series Class of Distributions: Properties and Applications

Nametso Dire, Broderick Oluyede, Thatayaone Moakofi*, Lesego Gabaitiri, Bakang Tlhaloganyang

Department of Mathematics and Statistical Sciences, Botswana International University of Science and Technology, Palapye, Botswana

Abstract Many standard lifetime distributions cannot jointly represent skewed observations, tail variation, and non-monotonic hazard rates, particularly when failure is generated by an unobserved random number of competing risks. This paper introduces the Topp-Leone modified Kies-G power series class of distributions to address these modelling problems. The class combines baseline-distribution selection, modified Kies-G odds transformation, Topp-Leone shape control, and zero-truncated power-series compounding through a random-minimum construction. General expressions are derived for the distribution, density, survival, hazard, quantile, moments, moment-generating function, Rényi entropy, and order statistics. Five estimation methods are examined through Monte Carlo simulations under two parameter settings and sample sizes ranging from from 25 to 800. The special case of TL-MK-LLoGP distribution is applied to acute bone cancer survival times, airborne-transceiver repair times, and bank customer waiting times and compared with five flexible four-parameter models. It produces the smallest reported AIC and BIC values across the three datasets, although the magnitude of improvement varies. The proposed class therefore provides an additional modelling option for positive data requiring latent-risk interpretation and flexible hazard-rate behaviour.

Keywords Topp-Leone generator; modified Kies-G family; power series distributions; hazard rate function; parameter estimation; risk measures

AMS 2010 subject classifications 62E99; 60E05

DOI: 10.19139/soic-2310-5070-4055

1. Introduction

The development of generalized classes and families of distributions through transformations or compounding has attracted a lot of attention in recent years. These methods enhance the flexibility of statistical modelling in different domains like economics, survival research, and reliability analysis. A wide range of hazard shapes including increasing, decreasing, bathtub, and upside-down bathtub shapes are intended to be captured by these new generalized distributions.

The Weibull-G family of distributions, first introduced by Bourguignon et al. (2014), is useful for lifetime and reliability analysis due to its ability to extend the classical Weibull distribution by incorporating a flexible baseline distribution function. This family is capable of modelling various shapes of the probability density function (PDF) and hazard rate function (HRF), including increasing, decreasing, bathtub, and upside-down bathtub forms. Its flexibility has led to widespread adoption in applications comprising survival data modelling and risk analysis.

Building upon the Weibull-G framework, several extensions and generalized families of distributions have been developed to further enhance modelling power and flexibility. These include new Weibull-G family of distributions

*Correspondence to: Thatayaone Moakofi (Email: thatayaone.moakofi@gmail.com). Department of Mathematics and Statistical Sciences, Botswana International University of Science and Technology, Palapye, BW.

ISSN 2310-5070 (online) ISSN 2311-004X (print)
Copyright © 2026 International Academic Press

by Tahir et al. (2016), gamma Weibull-G family of distributions by Oluyede et al. (2018), beta Marshall-Olkin-G family of distributions by Alizadeh et al. (2015), and Topp-Leone-Harris-G family of distributions by Oluyede et al. (2023), to mention just a few.

Recent research has continued to develop generator-based and power-series distributional classes for modelling complex density, hazard-rate, and tail behaviours. In power-series modelling, Gabanakgosi and Oluyede (2024) combined the Topp-Leone and Gompertz-G constructions with power-series compounding, Chamunorwa et al. (2024) developed a Type II exponentiated half-logistic-Gompertz-G power-series class, and Nkomo et al. (2024) introduced a Topp-Leone type I heavy-tailed-G power-series class. Related generator-based developments include the Marshall-Olkin-Topp-Leone-Gompertz-G family proposed by Oluyede et al. (2024), the Ristić-Balakrishnan heavy-tailed type II Topp-Leone-G family studied by Warahena-Liyanage et al. (2025), and the Topp-Leone modified Kies-G family developed by Swetha and Nagarjuna (2025). These studies provide the immediate theoretical foundation for the present work. The proposed TL-MK-GPS class of distributions extends this literature by introducing zero-truncated power-series compounding into the TL-MK-G construction, thereby allowing both the baseline distribution and the discrete compounding law to determine the resulting distributional behaviour.

Alongside these developments, the Topp–Leone-G (TL-G) family of distributions is another generator developed by Al-Shomrani et al. (2016), that has gained attention due to its flexibility and ability to model data with varying hazard functions. Given a baseline cumulative distribution function (CDF) $G(x;\psi)$, the CDF and PDF of the Topp-Leone-G family of distributions are

$$F_{TL-G}(x;\alpha,\psi) = \{1-[1-G(x;\psi)]^2\}^{\alpha}, \tag{1.1}$$

and

$$f_{TL-G}(x;\alpha,\psi) = 2\alpha g(x;\psi)[1-G(x;\psi)]\{1-[1-G(x;\psi)]^2\}^{\alpha-1}, \tag{1.2}$$

respectively, for $\alpha > 0$, where $g(x;\psi)$ is the baseline PDF with parameter vector ψ.

Furthermore, Al-Babtain et al. (2020), proposed a new family of distributions based on the modified Kies (MK) distribution using a T-X generator by Alzaatreh et al. (2013). The modified Kies-G (MK-G) family of distributions has emerged as a useful family that further generalizes baseline distributions by introducing a new parameter that modulate tail behavior and hazard shapes. The MK-G family transforms the baseline CDF in a way that offers additional flexibility in capturing non-monotonic hazard rates and diverse tail structures.

The CDF and PDF of the MK-G family of distributions are given by

$$F_{MK-G}(x;\beta,\psi) = 1-\exp\left\{-\left(\frac{G(x;\psi)}{1-G(x;\psi)}\right)^{\beta}\right\} \tag{1.3}$$

and

$$f_{MK-G}(x;\beta,\psi) = \frac{\beta g(x;\psi)G(x;\psi)^{\beta-1}}{[1-G(x;\psi)]^{\beta+1}}\exp\left\{-\left(\frac{G(x;\psi)}{1-G(x;\psi)}\right)^{\beta}\right\}, \tag{1.4}$$

respectively, for $\beta > 0$ and baseline parameter vector ψ.

The modified Kies-G family should be distinguished from the original Kies construction. The latter is a specific lifetime distribution, whereas the modified Kies-G family is generated by applying the modified Kies transformation to the baseline odds $G(x;\psi)/[1-G(x;\psi)]$. Consequently, the modified Kies-G family inherits the support and parameters of the selected baseline distribution, while β controls the modified Kies transformation (Al-Babtain et al. (2020)). In the present study, the Topp-Leone transformation is subsequently applied to this modified Kies-G family before introducing the power-series compounding mechanism. Combining Equations (1.1) and (1.2) with Equations (1.3) and (1.4), we obtain the Topp-Leone modified Kies-G (TL-MK-G) family of distributions developed by Swetha and Nagarjuna (2025) with CDF and PDF given as:

$$F_{TL-MK-G}(x;\alpha,\beta,\psi)=\left\{1-\exp\left[-2\left(\frac{G(x;\psi)}{1-G(x;\psi)}\right)^{\beta}\right]\right\}^{\alpha}, \tag{1.5}$$

and,

$$\begin{aligned} f_{TL-MK-G}(x;\alpha,\beta,\psi)=&\frac{2\alpha\beta g(x;\psi)G(x;\psi)^{\beta-1}}{[1-G(x;\psi)]^{\beta+1}}\exp\left[-2\left(\frac{G(x;\psi)}{1-G(x;\psi)}\right)^{\beta}\right]\\ &\times\left\{1-\exp\left\{-2\left(\frac{G(x;\psi)}{1-G(x;\psi)}\right)^{\beta}\right\}\right\}^{\alpha-1}, \end{aligned} \tag{1.6}$$

respectively for $\beta,\alpha>0$ and baseline parameter vector ψ.

Reliability, survival, and risk data may exhibit substantial skewness, heavy tails, and non-monotonic hazard rates, including bathtub and upside-down-bathtub shapes. A single conventional distribution may not represent these features simultaneously. The proposed construction addresses this modelling problem by combining three complementary mechanisms. The Topp-Leone generator provides additional control over distributional shape, the modified Kies-G transformation introduces flexibility in the tail and hazard-rate behaviour, and power-series compounding represents a random number of latent competing risks through the minimum of a zero-truncated number of independent lifetime variables. Their combination therefore provides a unified class from which models with different density, tail, and hazard-rate behaviours can be obtained.

The three components of the proposed class address different aspects of the modelling problem. The Topp-Leone generator provides additional control over distributional shape, while the modified Kies-G transformation changes the tail and hazard-rate behaviour through the odds of the baseline distribution. Power-series compounding introduces heterogeneity associated with a random number of latent competing causes, because the observed lifetime is represented as the minimum of a zero-truncated number of independent lifetime variables. The resulting TL-MK-GPS construction therefore combines continuous shape and tail modification with a discrete latent-count mechanism. This is relevant for positive lifetime and waiting-time data that may display skewness, complex hazard-rate behaviour, and unobserved variation in the number of potential causes.

The remainder of this paper is organized as follows. Section 2 introduces the TL-MK-GPS class of distributions and presents its formulation, including the hazard-rate shape characterization. Section 3 develops selected statistical properties of the proposed class, including the quantile function, sub-classes and sub-families, density expansion, moments, moment-generating function, Rényi entropy, and order statistics. Section 4 examines the convergence of the infinite-series expansions used in the theoretical development. Section 5 presents five methods for estimating the model parameters, including maximum likelihood, Anderson-Darling, ordinary least squares, weighted least squares, and Cramér-von Mises estimation. Section 6 presents the main power-series sub-classes, while Section 7 develops selected special cases based on specific baseline and power-series distributions. Section 8 reports the Monte Carlo simulation study used to assess the finite-sample performance of the estimation methods. Section 9 presents selected risk measures and their numerical evaluation. Section 10 applies the TL-MK-LLoGP model to three real datasets and compares its fit with competing distributions. Section 11 discusses the main findings and limitations of the study. Finally, Section 12 provides the concluding remarks.

2. The New Class of Distributions

In this section, we develop the Topp–Leone modified Kies-G power series (TL-MK-GPS) class of distributions. Let $X_1,X_2,\ldots,X_N$ be independent and identically distributed (i.i.d.) random variables from the TL-MK-G family of distributions. Let N be a discrete random variable following a power-series distribution truncated at zero, with

probability mass function given by

$$P(N=\nu)=\frac{a_\nu\theta^\nu}{C(\theta)},\qquad \nu=1,2,3,\ldots.$$

Here, $a_\nu>0$ is a sequence of positive real numbers, $\theta>0$, and

$$C(\theta)=\sum_{\nu=1}^{\infty}a_\nu\theta^\nu$$

is the finite normalizing function.

Given $N=\nu$, the conditional CDF of the minimum $X_{(1)}=\min(X_1,\ldots,X_\nu)$ is

$$F_{X_{(1)}|N=\nu}(x)=1-\left[1-F_{TL\text{-}MK\text{-}G}(x;\alpha,\beta,\psi)\right]^\nu=1-\left[\bar{F}_{TL\text{-}MK\text{-}G}(x;\alpha,\beta,\psi)\right]^\nu.$$

The marginal CDF of $X_{(1)}$ is

$$\begin{aligned}F_{X_{(1)}}(x)&=\sum_{\nu=1}^{\infty}P(N=\nu)F_{X_{(1)}|N=\nu}(x)\\&=\sum_{\nu=1}^{\infty}\frac{a_\nu\theta^\nu}{C(\theta)}\left[1-\left\{\bar{F}_{TL\text{-}MK\text{-}G}(x;\alpha,\beta,\psi)\right\}^\nu\right]\\&=1-\sum_{\nu=1}^{\infty}\frac{a_\nu\theta^\nu}{C(\theta)}\left[\bar{F}_{TL\text{-}MK\text{-}G}(x;\alpha,\beta,\psi)\right]^\nu.\end{aligned}\tag{2.1}$$

This representation holds for $\alpha,\beta,\theta>0$ and baseline parameter vector ψ. For notational convenience, define

$$T_G(x;\beta,\psi)=\left(\frac{G(x;\psi)}{1-G(x;\psi)}\right)^\beta.\tag{2.2}$$

Substituting the survival function of the TL-MK-G distribution into Equation (2.1) gives the CDF of the TL-MK-GPS class:

$$F_{TL-MK-GPS}(x;\alpha,\beta,\theta,\psi)=1-\frac{C\left(\theta\left[1-\left\{1-\exp\left(-2T_G(x;\beta,\psi)\right)\right\}^\alpha\right]\right)}{C(\theta)}.\tag{2.3}$$

The corresponding PDF is

$$\begin{aligned}f_{TL-MK-GPS}(x;\alpha,\beta,\theta,\psi)=&\frac{2\alpha\beta\theta g(x;\psi)[G(x;\psi)]^{\beta-1}}{C(\theta)[1-G(x;\psi)]^{\beta+1}}\exp\left[-2T_G(x;\beta,\psi)\right]\\&\times\left\{1-\exp\left[-2T_G(x;\beta,\psi)\right]\right\}^{\alpha-1}\\&\times C'\left(\theta\left[1-\left\{1-\exp\left[-2T_G(x;\beta,\psi)\right]\right\}^\alpha\right]\right).\end{aligned}\tag{2.4}$$

The survival function is

$$\bar{F}_{TL-MK-GPS}(x;\alpha,\beta,\theta,\psi)=\frac{C\left(\theta\left[1-\left\{1-\exp\left[-2T_G(x;\beta,\psi)\right]\right\}^\alpha\right]\right)}{C(\theta)},\tag{2.5}$$

and the hazard-rate function is

$$h_{TL-MK-GPS}(x;\alpha,\beta,\theta,\psi) = \frac{2\alpha\beta\theta g(x;\psi)[G(x;\psi)]^{\beta-1}}{[1-G(x;\psi)]^{\beta+1}} \times \frac{C'\left(\theta\left[1-\{1-\exp\left[-2T_G(x;\beta,\psi)\right]\}^{\alpha}\right]\right)}{C\left(\theta\left[1-\{1-\exp\left[-2T_G(x;\beta,\psi)\right]\}^{\alpha}\right]\right)} \times \{1-\exp\left[-2T_G(x;\beta,\psi)\right]\}^{\alpha-1}\exp\left[-2T_G(x;\beta,\psi)\right]. \tag{2.6}$$

These expressions hold for $\alpha, \beta, \theta > 0$ and baseline parameter vector ψ.

If the baseline distribution contains q free parameters, the general TL-MK-GPS class has $q+3$ free parameters: α, β, θ, and the q parameters contained in ψ. The number of parameters therefore depends on the selected baseline distribution. For the TL-MK-LLoGP special case, the log-logistic baseline has one parameter, c, so the model has four free parameters in the order $(\alpha, \beta, \theta, c)$. The simpler subfamilies presented in Table 3.1 can be used when the additional flexibility of the complete model is not required.

2.1. Hazard-Rate Shape Characterization

For a differentiable member of the TL-MK-GPS class, let $f(x)$, $\overline{F}(x)$, and $h(x) = f(x)/\overline{F}(x)$ denote its density, survival function, and hazard-rate function, respectively. Following the failure-rate characterization approach discussed by Glaser (1980), differentiation of the hazard-rate function gives

$$h'(x) = \frac{f'(x)\overline{F}(x) + f^2(x)}{\overline{F}^{\,2}(x)}. \tag{2.7}$$

Since $\overline{F}^{\,2}(x) > 0$, the shape of the hazard-rate function is determined by

$$\Delta(x) = f'(x)\overline{F}(x) + f^2(x). \tag{2.8}$$

The hazard rate is increasing when $\Delta(x) > 0$ and decreasing when $\Delta(x) < 0$. A change in sign from negative to positive produces a bathtub shape, whereas a change from positive to negative produces an upside-down-bathtub shape.

As the TL-MK-GPS class permits different baseline distributions and power-series normalizing functions, a single baseline-independent set of necessary and sufficient parameter restrictions for every hazard shape is not generally available. Nevertheless, the existence of the principal shapes can be demonstrated constructively through specific members and parameter combinations. For the TL-MK-LLoGP distribution in Figure 7.1, $(\alpha, \beta, \theta, c) = (4, 0.7, 1, 1.81)$ produces an increasing hazard rate, $(14, 0.2, 1.7, 0.07)$ produces a decreasing hazard rate, and $(1.9, 0.7, 8, 1.4)$ produces a bathtub-shaped hazard rate. For the TL-MK-LinLog distribution in Figure 7.3, $(\alpha, \beta, \theta, c) = (20, 0.3, 0.5, 3)$ produces an upside-down-bathtub hazard rate. These parameter combinations provide numerical counterexamples to the claim that the proposed class is restricted to a single monotonic hazard-rate form. They establish the existence of the stated shapes within the class, but do not imply that every baseline distribution produces all four shapes.

The use of explicit parameter combinations and graphical evaluations to establish the existence of different hazard-rate shapes is also consistent with recent lifetime-distribution studies (Al Mutairi et al. (2021)).

3. Some Statistical Properties

Statistical properties of the TL-MK-GPS class of distributions are discussed in this section. The quantile function, density expansion, moments, generating function, Rényi entropy and distribution of the order statistics are presented.

3.1. *Quantile Function*

The quantile function is particularly useful for producing random numbers from a given distribution. The quantile function $Q_{TL-MK-GPS}(p)$ of the TL-MK-GPS class of distributions is derived by using Equation (2.3) as follows:

$$p = 1 - \frac{C\left(\theta\left[1-\left\{1-\exp\left(-2\left(\frac{G(x;\psi)}{1-G(x;\psi)}\right)^{\beta}\right)\right\}^{\alpha}\right]\right)}{C(\theta)}, \quad 0 < p < 1,$$

so that,

$$\left\{-\frac{1}{2}\left\{\ln\left[1-\{1-\theta^{-1}C^{-1}\big((1-p)C(\theta)\big)\}^{\frac{1}{\alpha}}\right]\right\}\right\}^{\frac{1}{\beta}} = \frac{G(x;\psi)}{1-G(x;\psi)}.$$

The quantile function of the TL-MK-GPS class of distributions reduces to

$$Q_{TL-MK-GPS}(p) = G^{-1}\left(\frac{\left\{-\frac{1}{2}\left\{\ln\left[1-\{1-\theta^{-1}C^{-1}\big((1-p)C(\theta)\big)\}^{\frac{1}{\alpha}}\right]\right\}\right\}^{\frac{1}{\beta}}}{1+\left[\left\{-\frac{1}{2}\left\{\ln\left[1-\{1-\theta^{-1}C^{-1}\big((1-p)C(\theta)\big)\}^{\frac{1}{\alpha}}\right]\right\}\right\}^{\frac{1}{\beta}}\right]}\right), \tag{3.1}$$

for $0 < p < 1$. This quantile function will be used in Monte Carlo simulation studies to generate random numbers. It will also be used in a numerical study of risk measures for specified baseline CDF G, and power series distribution.

3.2. *Sub-classes and Sub-families of TL-MK-GPS Class of Distributions*

The following table presents sub-classes and sub-families of the TL-MK-GPS class of distributions under specific parameter constraints. These simplifications highlight the behavior of the model when one or more parameters take given values, revealing connections to sub-families such as the TL-MK-G and other simplified forms.

Parameters	**Sub-family/Sub-class**	**Simplified CDF Form** $F(x)$
$\beta = 1$	TL-MK-GPS (α, θ, ψ)	$1 - \frac{C\left(\theta\left[1-\left\{1-\exp\left(-2\left(\frac{G(x;\psi)}{1-G(x;\psi)}\right)\right)\right\}^{\alpha}\right]\right)}{C(\theta)}$
$\alpha = 1$	TL-MK-GPS (β, θ, ψ)	$1 - \frac{C\left(\theta\left[\exp\left(-2T_G(x;\beta,\psi)\right)\right]\right)}{C(\theta)}$
$\alpha = \beta = 1$	TL-MK-GPS (θ, ψ)	$1 - \frac{C\left(\theta\exp\left(-2\left(\frac{G(x;\psi)}{1-G(x;\psi)}\right)\right)\right)}{C(\theta)}$
$\theta \to 0^+$	TL-MK-G (α, β, ψ)	$\{1-\exp\left(-2T_G(x;\beta,\psi)\right)\}^{\alpha}$
$\theta \to 0^+,\ \beta = 1$	TL-MK-G (α, ψ)	$\left\{1-\exp\left(-2\left(\frac{G(x;\psi)}{1-G(x;\psi)}\right)\right)\right\}^{\alpha}$
$\theta \to 0^+,\ \alpha = 1$	TL-MK-G (β, ψ)	$1-\exp\left(-2T_G(x;\beta,\psi)\right)$
$\theta \to 0^+,\ \alpha = \beta = 1$	TL-MK-G (ψ)	$1-\exp\left(-2\left(\frac{G(x;\psi)}{1-G(x;\psi)}\right)\right)$

Table 3.1. Simplified forms of the TL-MK-GPS distributions under parameter constraints

The TL-MK-G(α, β, ψ), TL-MK-G(α, ψ), TL-MK-G(β, ψ) and TL-MK-G(ψ) sub-families can also be found in the paper by Swetha and Nagarjuna (2025).

3.3. Density Expansion

The linear representation of the PDF of the TL-MK-GPS class of distributions is derived using the power series expansion, generalized binomial expansion and exponential expansion. The generalised binomial and exponential expansions are $(1-x)^r = \sum_{n=0}^{\infty}(-1)^n\binom{r}{n}x^n$ for $|x|<1$ and $e^x = \sum_{n=0}^{\infty}\frac{x^n}{n!}$, respectively. Let $f_{TL-MK-GPS}(x;\alpha,\beta,\theta,\psi)$ be denoted by $f(x)$. Note that we can re-write the PDF in Equation (2.4) as follows:

$$f(x) = \frac{2\alpha\beta\theta g(x;\psi)(G(x;\psi))^{\beta-1}}{[1-G(x;\psi)]^{\beta+1}} \times \{1-\exp\left(-2T_G(x;\beta,\psi)\right)\}^{\alpha-1}\exp\left(-2T_G(x;\beta,\psi)\right) \times \sum_{n=1}^{\infty}\frac{na_n\theta^n}{C(\theta)}\left[1-\{1-\exp\left(-2T_G(x;\beta,\psi)\right)\}^{\alpha}\right]^{n-1}.$$

Now, using the generalised binomial expansions and exponential expansion given above, the PDF can be re-written as

$$f(x) = \frac{2\theta\alpha\beta}{C(\theta)}\sum_{n=1}^{\infty}\sum_{q,p,k,r,j,i=0}^{\infty}\frac{(-2)^k na_n\theta^n(p+1)^k(-1)^{q+p+j+i}}{(i+1)k!} \times \binom{n-1}{q}\binom{\alpha(q+1)-1}{p}\binom{\beta(k+1)+r}{r}\binom{\beta(k+1)+r-1}{j} \times \binom{j}{i}(i+1)g(x;\psi)G^i(x;\psi).$$

Consequently, the PDF of the TL-MK-GPS class of distributions can be expressed as

$$f(x) = \sum_{i=0}^{\infty}\delta_{i+1}h_{i+1}(x;\psi), \tag{3.2}$$

where

$$\delta_{i+1} = \frac{2\alpha\beta}{C(\theta)}\sum_{n=1}^{\infty}\sum_{q,p,k,r,j=0}^{\infty}\frac{(-2)^k na_n\theta^{n+1}(p+1)^k(-1)^{q+p+j+i}}{(i+1)k!} \tag{3.3}$$

$$\times \binom{n-1}{q}\binom{\alpha(q+1)-1}{p}\binom{\beta(k+1)+r}{r}\binom{\beta(k+1)+r-1}{j}\binom{j}{i} \tag{3.4}$$

$$\tag{3.5}$$

and $h_{i+1}(x;\psi) = (i+1)g(x;\psi)G^i(x;\psi)$ is an Exponentiated-G (Exp-G) density with power parameter $(i+1)$. This result shows that the PDF of the new class of distributions can be expressed as an infinite linear combination of the Exp-G densities. Clearly, the mathematical and statistical properties of the new class of distributions follows directly from those of the Exp-G distribution. **See appendix for details of the series expansion of the density function.**

The infinite-series representation is used for analytical derivations and is not used to evaluate the likelihood, CDF, PDF, or hazard function of the fitted special cases. The Poisson, geometric, logarithmic, binomial, and negative-binomial cases have closed-form normalizing functions; therefore, no numerical truncation or associated truncation error is involved in the simulation or real-data applications. The interchange and manipulation of the theoretical sums require absolute convergence. For a power-series member without a closed-form normalizing function, numerical implementation would require a stated truncation level and remainder tolerance.

3.4. Moments and Moment Generating Function

Given a random variable Y_{i+1} which follows Exp-G distribution with power parameter $(i+1)$, we obtain the r^{th} moment of the TL-MK-GPS class of distributions using Equation (3.2) as follows,

$$E(X^r) = \int_{-\infty}^{\infty} x^r f_{TL-MK-GPS}(x;\alpha,\beta,\theta,\psi)\,dx = \sum_{i=0}^{\infty} \delta_{i+1} E\left(Y_{i+1}^r\right), \tag{3.6}$$

where, $E(Y_{i+1}^r)$ is the r^{th} moment of an exponentiated-G random variable with power parameter $(i+1)$, and δ_{i+1} is defined in Equation (3.3). The moment generating function of the new class of distributions is,

$$M_X(t) = E(e^{tX}) = \sum_{i=0}^{\infty} \delta_{i+1} E(e^{tY_{i+1}}).$$

The existence of the r^{th} moment of the TL-MK-GPS distribution depends on the corresponding moments of the exponentiated-G components and the absolute convergence of the weighted series in Equation (3.6). Consequently, moment existence cannot be specified independently of the selected baseline distribution.

As $\theta \to 0^+$, the power-series compounding mechanism vanishes and the TL-MK-GPS distribution converges to the TL-MK-G subfamily reported in Table 3.1. Subject to the conditions required for interchanging the limit and integration, its r^{th} moment therefore converges to the corresponding moment of the TL-MK-G distribution. As $\alpha \to 0^+$, the distribution becomes concentrated near the lower endpoint of the baseline support. In contrast, large values of α shift probability toward the upper part of the support, so higher-order moments may become large or fail to exist when the baseline has unbounded support. As $\beta \to \infty$, the transformation becomes increasingly concentrated around the baseline median, whereas the limit $\beta \to 0^+$ is non-regular. These limiting cases explain why extreme parameter values require careful numerical treatment.

The model is identifiable for parameter values at which distinct parameter vectors produce distinct distribution functions and the observed information matrix is nonsingular. Nevertheless, weak identifiability may occur near $\theta = 0$, because the power-series component then has progressively less influence and the model approaches the non-compounded TL-MK-G subfamily. Numerical instability may also arise near the degenerating limits $\alpha \to 0^+$ and $\beta \to 0^+$ or for very large shape parameters. The profile log-likelihood plots in Figures 10.1, 10.4, and 10.7 show single maxima for the three fitted datasets, providing dataset-specific evidence of identifiability at the reported estimates. These plots do not, however, establish global identifiability over the entire parameter space.

3.5. Rényi Entropy

An entropy quantifies the uncertainty associated with a random variable X characterized by the PDF $f(x)$. Rényi entropy is a generalization of Shannon entropy. This allows for a broader understanding of uncertainty in probability distributions beyond the traditional Shannon framework. The Rényi entropy is defined by

$$I_\xi(X) = \frac{1}{1-\xi} \log\left(\int_{-\infty}^{\infty} f^\xi(x)\,dx\right), \quad \xi > 0 \text{ and } \xi \neq 1.$$

Note that

$$\begin{aligned} f^\xi(x) = [2\alpha\beta\theta g(x;\psi)]^\xi \frac{(G(x;\psi))^{\xi(\beta-1)}}{[1-G(x;\psi)]^{\xi(\beta+1)}} \exp\left(-2\xi T_G(x;\beta,\psi)\right) \\ \times \{1-\exp\left(-2T_G(x;\beta,\psi)\right)\}^{\xi(\alpha-1)} \\ \times \left\{\frac{C'\left(\theta\left[1-\{1-\exp\left(-2T_G(x;\beta,\psi)\right)\}^\alpha\right]\right)}{C(\theta)}\right\}^\xi. \end{aligned}$$

We can re-write the $f^{\xi}(x)$ as follows:

$$f^{\xi}(x) = [2\alpha\beta\theta g(x;\psi)]^{\xi} \frac{(G(x;\psi))^{\xi(\beta-1)}}{[1-G(x;\psi)]^{\xi(\beta+1)}} \exp\left(-2\xi\left(\frac{G(x;\psi)}{1-G(x;\psi)}\right)^{\beta}\right) \times \left\{1-\exp\left(-2\left(\frac{G(x;\psi)}{1-G(x;\psi)}\right)^{\beta}\right)\right\}^{\xi(\alpha-1)} \times \sum_{q=0}^{\infty} b_n^q d_{q,\xi} \left[1-\left\{1-\exp\left(-2\left[\frac{G(x;\psi)}{1-G(x;\psi)}\right]^{\beta}\right)\right\}^{\alpha}\right]^{q(n-1)},$$

where, $b_n^q = \left[\sum_{n=1}^{\infty} \frac{a_n \theta^{n-1}}{C(\theta)}\right]^q$, $d_{q,\xi} = (qb_0)^{-1} \sum_{h=1}^{q} [q(h+1)-q]\, b_h d_{q-h,\xi}$, and $d_{0,\xi} = b_0^{\xi}$.

Consequently, Renyi entropy for TL-MK-GPS class of distributions reduces to

$$I_{\xi}(X) = \frac{1}{1-\xi} \log\left(\sum_{w=0}^{\infty} \vartheta_w e^{(1-\xi)I_{REG}}\right), \quad \xi > 0 \text{ and } \xi \neq 1,$$

where

$$\vartheta_w = \left[\frac{2\alpha\beta\theta}{C(\theta)}\right]^{\xi} \sum_{q,r,s,t,u,v=0}^{\infty} \frac{(-2)^t (s+\xi)^t b_n^q d_{q,\xi} (-1)^{r+s+v+w}}{\left(\frac{w}{\xi}+1\right)^{\xi} t!} \times \binom{q}{r} \binom{\alpha r + \xi(\alpha-1)}{s} \binom{\beta t + \xi(\beta+1) + u - 1}{u} \times \binom{u + \beta t + \xi(\beta-1)}{v} \binom{v}{w},$$

and

$$I_{REG} = \frac{1}{1-\xi} \log \int_0^{\infty} \left(\left(\frac{w}{\xi}+1\right) g(x;\psi) G^{\frac{w}{\xi}}(x;\psi)\right)^{\xi} dx$$

is the Rényi entropy of Exp-G density with power parameter $(\frac{w}{\xi}+1)$.

3.6. Order Statistics

Order statistics are fundamental in probability and statistics, with wide-ranging applications in areas such as reliability theory and quality control testing in engineering. Consider a sequence of independent and identically distributed random variables $X_1, X_2, \ldots, X_n$ drawn from the TL-MK-GPS class of distributions, the PDF of the i^{th} order statistic from the TL-MK-GPS class of distributions can be expressed as

$$f_{i:m}(x) = \frac{m!}{(i-1)!(m-i)!} \sum_{j=0}^{m-i} (-1)^j \binom{m-i}{j} f(x)[F(x)]^{j+i-1}.$$

Let the CDF $F_{TL-MK-GPS}(x;\alpha,\beta,\theta,\psi)$ and PDF $f_{TL-MK-GPS}(x;\alpha,\beta,\theta,\psi)$ be denoted by $F(x)$ and $f(x)$, respectively. Note that

$$[F(x)]^{j+i-1} = \left\{1 - \frac{C\left(\theta\left[1-\left\{1-\exp\left(-2\left(\frac{G(x;\psi)}{1-G(x;\psi)}\right)^{\beta}\right)\right\}^{\alpha}\right]\right)}{C(\theta)}\right\}^{j+i-1}$$
$$= \sum_{k=0}^{\infty}(-1)^k\binom{j+i-1}{k}\left\{\frac{C\left(\theta\left[1-\left\{1-\exp\left(-2T_G(x;\beta,\psi)\right)\right\}^{\alpha}\right]\right)}{C(\theta)}\right\}^{k}.$$

The PDF of the i^{th} order statistic can be written as

$$f_{i:n}(x) = \frac{2m!\alpha\beta g(x;\psi)\left(G(x;\psi)\right)^{\beta-1}}{(i-1)!(m-i)![1-G(x;\psi)]^{\beta+1}}$$
$$\times \sum_{j=0}^{m-i}\sum_{k=0}^{\infty}\sum_{l,n=1}^{\infty}\frac{na_n\theta^{n+l}e_{l,k}(-1)^{j+k}}{C^{k+1}(\theta)}\binom{m-i}{j}\binom{j+i-1}{k}$$
$$\times \exp\left(-2T_G(x;\beta,\psi)\right)\left\{1-\exp\left(-2T_G(x;\beta,\psi)\right)\right\}^{\alpha-1}$$
$$\times \left\{1-\left[1-\exp\left(-2T_G(x;\beta,\psi)\right)\right]^{\alpha}\right\}^{n-1}$$
$$\times \left\{1-\left[1-\exp\left(-2T_G(x;\beta,\psi)\right)\right]^{\alpha}\right\}^{l},$$

where, $e_{l,k} = (lb_0)^{-1}\sum_{h=1}^{l}\left[l(h+1)-l\right]b_h e_{l-h,k}$, and $e_{0,k} = b_0^k$.

Now following the same steps leading to Equation (3.2), the PDF of the i^{th} order statistic as can be written as

$$f_{i:n}(x) = \sum_{t=0}^{\infty}\phi_{t+1}h_{t+1}(x;\psi),$$

where $h_{t+1}(x;\psi) = (t+1)g(x;\psi)G^t(x;\psi)$ is an Exp-G density with power parameter $(t+1)$, and

$$\phi_{t+1} = \frac{2\alpha\beta m!}{C^{k+1}(\theta)(i-1)!(m-i)!}$$
$$\times \sum_{j=0}^{m-i}\sum_{k,w,p,q,r,s=0}^{\infty}\sum_{l,n=1}^{\infty}\frac{(-2)^q(p+1)^q na_n\theta^{n+l}e_{l,k}(-1)^{j+k+w+p+q+r+s+t}}{(t+1)q!}$$
$$\times \binom{m-i}{j}\binom{j+i-1}{k}\binom{l+n-1}{w}\binom{\alpha(w+1)-1}{p}\binom{\beta(q+1)+r}{r}$$
$$\times \binom{\beta(q+1)+r-1}{s}\binom{s}{t}.$$

4. Infinite Series Convergence

Series convergence are presented in this subsection.

4.1. First Series Expansion

Note that

$$C'\left(\theta\left[1-\left\{1-\exp\left(-2\left(\frac{G(x_i;\psi)}{\bar{G}(x_i;\psi)}\right)^{\beta}\right)\right\}^{\alpha}\right]\right)=\sum_{\nu=1}^{\infty}\nu a_{\nu}\theta^{\nu-1}\left[1-\left\{1-\exp\left(-2\left(\frac{G(x_i;\psi)}{\bar{G}(x_i;\psi)}\right)^{\beta}\right)\right\}^{\alpha}\right]^{\nu-1}.$$

Using the ratio test, we get

$$\begin{aligned}&\lim_{\nu\to\infty}\frac{(\nu+1)\,a_{\nu+1}\theta^{\nu}\left[1-\left\{1-\exp\left(-2\left(\frac{G(x_i;\psi)}{\bar{G}(x_i;\psi)}\right)^{\beta}\right)\right\}^{\alpha}\right]^{\nu}}{\nu a_{\nu}\theta^{\nu-1}\left[1-\left\{1-\exp\left(-2\left(\frac{G(x_i;\psi)}{\bar{G}(x_i;\psi)}\right)^{\beta}\right)\right\}^{\alpha}\right]^{\nu-1}}\\&=\lim_{\nu\to\infty}\frac{(\nu+1)a_{\nu+1}\theta}{\nu a_{\nu}}\left[1-\left\{1-\exp\left(-2\left(\frac{G(x_i;\psi)}{\bar{G}(x_i;\psi)}\right)^{\beta}\right)\right\}^{\alpha}\right].\end{aligned}$$

Since $\left\{1-\exp\left(-2\left(\frac{G(x_i;\psi)}{\bar{G}(x_i;\psi)}\right)^{\beta}\right)\right\}^{\alpha}$ is a cdf, we have

$$0<\left[1-\left\{1-\exp\left(-2\left(\frac{G(x_i;\psi)}{\bar{G}(x_i;\psi)}\right)^{\beta}\right)\right\}^{\alpha}\right]<1.$$

Note that

$$\lim_{\nu\to\infty}\frac{\nu+1}{\nu}=1,$$

and assuming that the power series coefficients satisfy

$$\lim_{\nu\to\infty}\frac{a_{\nu}+1}{a_{\nu}}=b<\infty,$$

where $b\geq 0$, then the ratio test implies convergence provided that

$$\theta b\left[1-\left\{1-\exp\left(-2\left(\frac{G(x_i;\psi)}{\bar{G}(x_i;\psi)}\right)^{\beta}\right)\right\}^{\alpha}\right]<1.$$

4.2. Second Series Expansion

Consider the term

$$\left[1-\left\{1-\exp\left[-2T_G(x;\beta,\psi)\right]\right\}^{\alpha}\right]^{n-1}.$$

Using the binomial expansion,

$$\left[1-\left\{1-\exp\left[-2T_G(x;\beta,\psi)\right]\right\}^{\alpha}\right]^{n-1}=\sum_{q=0}^{n-1}(-1)^q\binom{n-1}{q}\left\{1-\exp\left[-2T_G(x;\beta,\psi)\right]\right\}^{\alpha q}.$$

Since the density also contains

$$\left\{1-\exp\left[-2T_G(x;\beta,\psi)\right]\right\}^{\alpha-1},$$

we obtain

$$\{1-\exp\left[-2T_G(x;\beta,\psi)\right]\}^{\alpha-1}\{1-\exp\left[-2T_G(x;\beta,\psi)\right]\}^{\alpha q} = \{1-\exp\left[-2T_G(x;\beta,\psi)\right]\}^{\alpha(q+1)-1}.$$

Therefore, the generalized binomial expansion,

$$\{1-\exp\left[-2T_G(x;\beta,\psi)\right]\}^{\alpha(q+1)-1} = \sum_{p=0}^{\infty}(-1)^p\binom{\alpha(q+1)-1}{p}\{\exp\left[-2T_G(x;\beta,\psi)\right]\}^p.$$

Using the ratio test,

$$\lim_{p\to\infty}\left|\frac{\binom{\alpha(q+1)-1}{p+1}}{\binom{\alpha(q+1)-1}{p}}\right|\exp\left[-2T_G(x;\beta,\psi)\right] = \lim_{p\to\infty}\left|\frac{\alpha(q+1)-p-1}{p+1}\right|\exp\left[-2T_G(x;\beta,\psi)\right] = \exp\left[-2T_G(x;\beta,\psi)\right] < 1.$$

Thus, the second series converges for every x such that $0 < G(x;\psi) < 1$.

4.3. Third Series Expansion

From the second series expansion, we have the product

$$\begin{aligned}&\exp\left[-2T_G(x;\beta,\psi)\right]\exp\left[-2pT_G(x;\beta,\psi)\right]\\ &= \exp\left[-2T_G(x;\beta,\psi)-2pT_G(x;\beta,\psi)\right]\\ &= \exp\left[-2(p+1)T_G(x;\beta,\psi)\right].\end{aligned}$$

Using the exponential expansion

$$e^z = \sum_{k=0}^{\infty}\frac{z^k}{k!},$$

we obtain

$$\begin{aligned}\exp\left[-2(p+1)T_G(x;\beta,\psi)\right] &= \sum_{k=0}^{\infty}\frac{\left[-2(p+1)T_G(x;\beta,\psi)\right]^k}{k!}\\ &= \sum_{k=0}^{\infty}\frac{(-2)^k(p+1)^k}{k!}\left[T_G(x;\beta,\psi)\right]^k.\end{aligned}$$

Using the ratio test, we have

$$\lim_{k\to\infty}\frac{\frac{\left[-2(p+1)T_G(x;\beta,\psi)\right]^{k+1}}{(k+1)!}}{\frac{\left[-2(p+1)T_G(x;\beta,\psi)\right]^k}{k!}} = \lim_{k\to\infty}\frac{-2(p+1)T_G(x;\beta,\psi)}{k+1} = 0.$$

Thus, the series converges for every x such that $0 < G(x;\psi) < 1$.

5. Parameter Estimation Methods

In this section, we discuss different methods for estimating the unknown parameters of the TL-MK-GPS class of distributions. The estimation methods include Maximum Likelihood (ML), Ordinary Least Squares (OLS), Anderson-Darling (AD), Weighted Least Squares (WLS) and Cramér-Von Mises (CVM).

5.1. Maximum Likelihood Estimation

Let $X \sim TL-MK-GPS(\alpha,\beta,\theta,\psi)$ and $\Delta=(\alpha,\beta,\theta,\psi)^T$ be the vector of the model parameters. The log-likelihood function $\ell_n=\ell(\Delta)$ based on a random sample of size n from the TL-MK-GPS class of distributions is given by

$$\begin{aligned}\ell_n &= n\log(2\alpha\beta\theta)+\sum_{i=1}^{n}\log(g(x_i;\psi))+(\beta-1)\sum_{i=1}^{n}\log(G(x_i;\psi))\\ &-\sum_{i=1}^{n}\log(C(\theta))-(\beta+1)\sum_{i=1}^{n}\log(\bar{G}(x_i;\psi))\\ &-2\sum_{i=1}^{n}\left[\frac{G(x_i)}{\bar{G}(x_i;\psi)}\right]^{\beta}+(\alpha-1)\sum_{i=1}^{n}\log\left\{1-\exp\left(-2\left(\frac{G(x_i;\psi)}{\bar{G}(x_i;\psi)}\right)^{\beta}\right)\right\}\\ &+\sum_{i=1}^{n}\log\left\{C'\left(\theta\left[1-\left\{1-\exp\left(-2\left(\frac{G(x_i;\psi)}{\bar{G}(x_i;\psi)}\right)^{\beta}\right)\right\}^{\alpha}\right]\right)\right\}.\end{aligned}$$

To obtain the estimates of the unknown parameters from the TL-MK-GPS class of distributions we solve the nonlinear equation $U=(\frac{\partial\ell_n}{\partial\alpha},\frac{\partial\ell_n}{\partial\beta},\frac{\partial\ell_n}{\partial\theta},\frac{\partial\ell_n}{\partial\psi})^T=\mathbf{0}$, using a numerical method like Newton-Raphson procedure. **The elements of the score vector U are given in the appendix.**

The Fisher information matrix for the parameter vector $\boldsymbol{\Delta}=(\alpha,\beta,\theta,\boldsymbol{\psi})^T$ is defined by

$$\mathcal{I}(\boldsymbol{\Delta})=-\mathbb{E}\left[\frac{\partial^2\ell_n(\boldsymbol{\Delta})}{\partial\boldsymbol{\Delta}\,\partial\boldsymbol{\Delta}^T}\right]. \tag{5.1}$$

Equivalently, the observed information matrix is

$$\mathcal{J}(\boldsymbol{\Delta})=-\frac{\partial^2\ell_n(\boldsymbol{\Delta})}{\partial\boldsymbol{\Delta}\,\partial\boldsymbol{\Delta}^T}. \tag{5.2}$$

For the special cases considered in this study, where the baseline distribution contains a single parameter ψ, the observed information matrix is

$$\mathcal{J}(\boldsymbol{\Delta})=-\begin{pmatrix}\frac{\partial^2\ell_n}{\partial\alpha^2} & \frac{\partial^2\ell_n}{\partial\alpha\partial\beta} & \frac{\partial^2\ell_n}{\partial\alpha\partial\theta} & \frac{\partial^2\ell_n}{\partial\alpha\partial\psi}\\ \frac{\partial^2\ell_n}{\partial\beta\partial\alpha} & \frac{\partial^2\ell_n}{\partial\beta^2} & \frac{\partial^2\ell_n}{\partial\beta\partial\theta} & \frac{\partial^2\ell_n}{\partial\beta\partial\psi}\\ \frac{\partial^2\ell_n}{\partial\theta\partial\alpha} & \frac{\partial^2\ell_n}{\partial\theta\partial\beta} & \frac{\partial^2\ell_n}{\partial\theta^2} & \frac{\partial^2\ell_n}{\partial\theta\partial\psi}\\ \frac{\partial^2\ell_n}{\partial\psi\partial\alpha} & \frac{\partial^2\ell_n}{\partial\psi\partial\beta} & \frac{\partial^2\ell_n}{\partial\psi\partial\theta} & \frac{\partial^2\ell_n}{\partial\psi^2}\end{pmatrix}. \tag{5.3}$$

Evaluated at the maximum likelihood estimate $\widehat{\boldsymbol{\Delta}}$, the estimated variance-covariance matrix is obtained from the inverse observed information matrix as

$$\widehat{\mathrm{Var}}\left(\widehat{\boldsymbol{\Delta}}\right)=\mathcal{J}^{-1}\left(\widehat{\boldsymbol{\Delta}}\right). \tag{5.4}$$

Thus, the approximate standard errors of the maximum likelihood estimates are obtained from the square roots of the diagonal elements of $\mathcal{J}^{-1}(\widehat{\boldsymbol{\Delta}})$.

Under the usual regularity conditions,

$$\widehat{\boldsymbol{\Delta}}\overset{a}{\sim}N_{p+3}\left(\boldsymbol{\Delta},\mathcal{I}^{-1}(\boldsymbol{\Delta})\right). \tag{5.5}$$

Consequently, an approximate $100(1-\gamma)\%$ confidence interval for the j^{th} parameter Δ_j is

$$\widehat{\Delta}_j \pm z_{\gamma/2}\sqrt{\left[\mathcal{J}^{-1}\left(\widehat{\boldsymbol{\Delta}}\right)\right]_{jj}}, \tag{5.6}$$

where $z_{\gamma/2}$ is the corresponding standard normal critical value.

The nonlinear estimating equations for the five estimation methods were solved using the `nlminb` numerical optimization routine in R. The same optimization structure was used for maximum likelihood, Anderson–Darling, ordinary least squares, weighted least squares, and Cramér–von Mises estimation, with the corresponding objective function substituted for each method.

In the Monte Carlo study, the optimizer was initialized at the parameter vector used to generate the data. A lower bound of 0.01 was imposed on every parameter to preserve positivity, while no finite upper bound was imposed. An estimated parameter vector was retained only when `nlminb` returned convergence code zero. If this condition was not satisfied, the simulation and estimation step was repeated. Consequently, all estimates used to calculate the reported bias and RMSE values were obtained from successfully converged optimization runs.

The program did not retain the number of unsuccessful optimization attempts that occurred before the required number of converged estimates was obtained. A numerical non-convergence rate therefore cannot be reported retrospectively, and the simulation results should be interpreted as conditional on successful convergence. Recording both successful and unsuccessful attempts would provide a more complete assessment of numerical stability in future studies.

For the real-data applications, the profile log-likelihood plots in Figures 10.1, 10.4, and 10.7 display single interior maxima for the reported maximum-likelihood estimates. These plots provide dataset-specific evidence against competing local maxima at the fitted solutions, although they do not establish global convergence for every possible starting vector or dataset.

5.2. Anderson-Darling Estimation

The Anderson–Darling estimates (ADEs) are computed by minimizing the Anderson–Darling criterion function:

$$A\left(\Delta\right) = -n - \frac{1}{n}\sum_{i=1}^{n}\left(2i-1\right)\left[\log\left(F(x_{(i)};\alpha,\beta,\theta,\psi)\right) + \log\left(S(x_{(i)};\alpha,\beta,\theta,\psi)\right)\right],$$

where $F(x_{(i)};\alpha,\beta,\theta,\psi)$ and $S(x_{(i)};\alpha,\beta,\theta,\psi)$ represent the CDF and survival function of the i^{th} order statistic from the TL-MK-GPS class of distributions, respectively. Alternatively, the minimization can be approached by solving a system of nonlinear equations derived from the partial derivatives of the objective function with respect to each parameter, as shown below

$$\sum_{i=1}^{n}\left(2i-1\right)\left[\frac{\vartheta_z\left(x_{(i)};\alpha,\beta,\theta,\psi\right)}{F(x_{(i)};\alpha,\beta,\theta,\psi)} - \frac{\vartheta_z\left(x_{n+1-i};\alpha,\beta,\theta,\psi\right)}{S\left(x_{n+1-i};\alpha,\beta,\theta,\psi\right)}\right] = 0, z = 1,2,3,4,$$

where

$$\vartheta_1\left(x_{(i)};\alpha,\beta,\theta,\psi\right) = \frac{\partial F\left(x_{(i)};\alpha,\beta,\theta,\psi\right)}{\partial\alpha}, \tag{5.7}$$

$$\vartheta_2\left(x_{(i)};\alpha,\beta,\theta,\psi\right) = \frac{\partial F\left(x_{(i)};\alpha,\beta,\theta,\psi\right)}{\partial\beta}, \tag{5.8}$$

$$\vartheta_3\left(x_{(i)};\alpha,\beta,\theta,\psi\right) = \frac{\partial F\left(x_{(i)};\alpha,\beta,\theta,\psi\right)}{\partial\theta}, \tag{5.9}$$

and

$$\vartheta_4\left(x_{(i)};\alpha,\beta,\theta,\psi\right)=\frac{\partial F\left(x_{(i)};\alpha,\beta,\theta,\psi\right)}{\partial\psi_k}, \tag{5.10}$$

for $k=1,2,...,p$, and p is the number of parameters in the baseline parameter vector ψ.

5.3. Ordinary Least Squares Estimation

The OLS method estimates the parameters of the TL-MK-GPS class of distributions by minimizing the sum of squared deviations between the theoretical and empirical CDF values. The objective function is

$$V\left(\Delta\right)=\sum_{i=1}^{n}\left[F\left(x_{(i)};\alpha,\beta,\theta,\psi\right)-\frac{i}{n+1}\right]^2.$$

The OLS estimates (OLSEs) can be obtained by solving the non-linear equations:

$$\sum_{i=1}^{n}\left[F\left(x_{(i)};\alpha,\beta,\theta,\psi\right)-\frac{i}{n+1}\right]\vartheta_z\left(x_{(i)};\alpha,\beta,\theta,\psi\right)=0, z=1,2,3,4,$$

where $\vartheta_z\left(x_{(i)};\alpha,\beta,\theta,\psi\right)$ are defined in Equations (5.7), (5.8), (5.9) and (5.10).

5.4. Weighted Least Squares Estimation

The WLS method is a modified version of OLS where each term is weighted to give more importance to central observations. The WLS criterion function is

$$W\left(\Delta\right)=\sum_{i=1}^{n}\frac{(n+1)^2(n+2)}{i(n-1+1)}\left[F\left(x_{(i)};\alpha,\beta,\theta,\psi\right)-\frac{i}{n+1}\right]^2.$$

The WLS estimates (WLSEs) of the parameters of the TL-MK-GPS class of distributions are obtained by solving the non-linear equations:

$$\sum_{i=1}^{n}\frac{(n+1)^2(n+2)}{i(n-1+1)}\left[F\left(x_{(i)};\alpha,\beta,\theta,\psi\right)-\frac{i}{n+1}\right]\vartheta_z\left(x_{(i)};\alpha,\beta,\theta,\psi\right)=0, z=1,2,3,4,$$

where $\vartheta_z\left(x_{(i)};\alpha,\beta,\theta,\psi\right)$ are defined in Equations (5.7), (5.8), (5.9) and (5.10).

5.5. Cramér-von Mises Estimation

The CVM estimates (CVMEs) of the parameters of the TL-MK-GPS class of distributions are obtained through the minimization of the function

$$C\left(\Delta\right)=\frac{1}{12n}+\sum_{i=1}^{n}\left[F\left(x_{(i)};\alpha,\beta,\theta,\psi\right)-\frac{2i-1}{2n}\right]^2,$$

with respect to α,β,θ and parameter vector ψ. The CVMEs can also be obtained by solving the non-linear equations

$$\sum_{i=1}^{n}\left[F\left(x_{(i)};\alpha,\beta,\theta,\psi\right)-\frac{2i-1}{2n}\right]\vartheta_z\left(x_{(i)};\alpha,\beta,\theta,\psi\right)=0, z=1,2,3,4,$$

where $\vartheta_z\left(x_{(i)};\alpha,\beta,\theta,\psi\right)$ are defined in Equations (5.7), (5.8), (5.9) and (5.10).

6. Special Classes of the TL-MK-GPS Class of Distributions

We specify the power series distributions as Poisson, geometric, logarithmic, binomial and negative binomial to obtain the classes of distributions presented in the table below.

Distribution	a_n	$C(\theta)$	**Admissible Range for** θ	**CDF:** $F(x;\alpha,\beta,\theta,\psi)$
TL-MK-G Poisson	$\frac{1}{n!}$	$e^{\theta}-1$	$\theta>0$	$1-\frac{\exp\left(\theta\left[1-\{1-\exp\left(-2T_G(x;\beta,\psi)\right)\}^{\alpha}\right]\right)-1}{\exp(\theta)-1}$
TL-MK-G Geometric	1	$\frac{\theta}{1-\theta}$	$0<\theta<1$	$1-\frac{(1-\theta)\left[1-\{1-\exp\left(-2T_G(x;\beta,\psi)\right)\}^{\alpha}\right]}{\left(1-\theta\left[1-\{1-\exp\left(-2T_G(x;\beta,\psi)\right)\}^{\alpha}\right]\right)}$
TL-MK-G Logarithmic	$\frac{1}{n}$	$-\log(1-\theta)$	$0<\theta<1$	$1-\frac{\log\left(1-\theta\left[1-\{1-\exp\left(-2T_G(x;\beta,\psi)\right)\}^{\alpha}\right]\right)}{\log(1-\theta)}$
TL-MK-G Binomial	$\binom{m}{n}$	$(1+\theta)^m-1$	$\theta>0$	$1-\frac{\left(1+\theta\left[1-\{1-\exp\left(-2T_G(x;\beta,\psi)\right)\}^{\alpha}\right]\right)^m-1}{(1+\theta)^m-1}$
TL-MK-G Negative Binomial	$\binom{n+k-1}{n}$	$(1-\theta)^{-k}-1$	$0<\theta<1$	$1-\frac{\left(1-\theta\left[1-\{1-\exp\left(-2T_G(x;\beta,\psi)\right)\}^{\alpha}\right]\right)^{-k}-1}{(1-\theta)^{-k}-1}$

Table 6.1. Sub-classes of the TL-MK-GPS Class of Distributions

The five power-series distributions considered above are representative choices rather than an exhaustive set. They provide bounded and unbounded latent-count mechanisms with different levels of count variability. The general zero-truncated power-series formulation, together with several of its important members, is discussed by Osatohanmwen et al. (2020). Recent generator-based power-series models have also employed these discrete compounding mechanisms to produce flexible density, survival, and hazard-rate shapes (Gabanakgosi and Oluyede (2024); Chamunorwa et al. (2024); Nkomo et al. (2024)). Other zero-truncated discrete distributions may therefore be incorporated into the proposed TL-MK-GPS construction whenever their normalizing function $C(\theta)$ is finite and analytically tractable.

7. Special Cases

In this section, we specify the baseline distribution as well as the power series distribution to obtain some special cases of the new class of distributions. The special cases of the TL-MK-GPS are considered when the power series distribution is the Poisson, logarithmic and geometric distributions. The baseline CDFs that were considered include log-logistic, Lindley and uniform distribution, respectively. **Other special cases with baselines including exponential, Weibull and Kumaraswamy distributions can be found in the appendix.**

The three special cases were selected to demonstrate how different baseline supports and power-series compounding distributions affect the resulting model. Their selection should be guided by the support of the observed data, the empirical hazard-rate shape, and the required tail behaviour.

The TL-MK-LLoGP distribution combines a log-logistic baseline with Poisson compounding. It is defined on the positive real line and can represent increasing, decreasing, bathtub, and other non-monotonic hazard-rate forms. Related log-logistic power-series models have been applied to positive lifetime data (Nkomo et al. (2024); Oluyede et al. (2022)). The TL-MK-LLoGP model is therefore a suitable candidate for survival, reliability, and waiting-time data exhibiting similar characteristics.

The TL-MK-LinLog distribution uses a Lindley baseline and logarithmic compounding. Lindley-based power-series constructions have been used for lifetime and medical data modelling (Hassan et al. (2020)). This special case is relevant when the Lindley baseline is appropriate but additional flexibility in the density and hazard-rate shapes is required.

The TL-MK-UG distribution combines a uniform baseline with geometric compounding. The uniform baseline provides bounded support, while the geometric distribution is an established member of the zero-truncated power-series family (Osatohanmwen et al. (2020)). This special case is therefore suitable for variables with a known finite range, while retaining flexibility in the resulting hazard-rate shape.

7.1. Topp-Leone Modified Kies-Log-Logistic Poisson (TL-MK-LLoGP) Distribution

Considering the baseline distribution as the log-logistic distribution with CDF and PDF are given by $G(x;c) = 1-(1+x^c)^{-1}$ and $g(x;c) = cx^{c-1}(1+x^c)^{-2}$, respectively, for $x>0$ and $c>0$. Using Equations (2.3), (2.4) and (2.6), the CDF, PDF and HRF of the TL-MK-LLoGP distribution are given by

$$F_{TL-MK-LLP}(x;\alpha,\beta,\theta,c) = 1 - \frac{\exp\left(\theta\left[1-\{1-\exp\left(-2T_{LLoG}(x;\beta,c)\right)\}^{\alpha}\right]\right)-1}{\exp(\theta)-1},$$

$$\begin{aligned} f_{TL-MK-LLP}(x;\alpha,\beta,\theta,c) = {} & \frac{2\alpha\beta\theta[cx^{c-1}(1+x^c)^{-2}][1-(1+x^c)^{-1}]^{\beta-1}}{[\exp(\theta)-1][(1+x^c)^{-1}]^{\beta+1}} \\ & \times \exp\left(\theta\left[1-\{1-\exp\left(-2T_{LLoG}(x;\beta,c)\right)\}^{\alpha}\right]\right) \\ & \times \{1-\exp\left(-2T_{LLoG}(x;\beta,c)\right)\}^{\alpha-1} \\ & \times \exp\left(-2T_{LLoG}(x;\beta,c)\right), \end{aligned}$$

and

$$\begin{aligned} h_{TL-MK-LLP}(x;\alpha,\beta,\theta,c) = {} & \frac{2\alpha\beta\theta[cx^{c-1}(1+x^c)^{-2}][1-(1+x^c)^{-1}]^{\beta-1}}{[(1+x^c)^{-1}]^{\beta+1}} \\ & \times \frac{\exp\left(\theta\left[1-\{1-\exp\left(-2T_{LLoG}(x;\beta,c)\right)\}^{\alpha}\right]\right)}{\exp\left(\theta\left[1-\{1-\exp\left(-2T_{LLoG}(x;\beta,c)\right)\}^{\alpha}\right]\right)-1} \\ & \times \{1-\exp\left(-2T_{LLoG}(x;\beta,c)\right)\}^{\alpha-1} \\ & \times \exp\left(-2T_{LLoG}(x;\beta,c)\right) \end{aligned}$$

respectively for $x,\alpha,\beta,\theta,c>0$, where

$$T_{LLoG}(x;\beta,c) = \left(\frac{1-(1+x^c)^{-1}}{(1+x^c)^{-1}}\right)^{\beta}.$$

Figure 7.1 presents the PDF and HRF of the TL-MK-LLoGP distribution for selected parameter combinations. The PDF exhibits unimodal, reverse-J, J-shaped, right-skewed, and left-skewed forms. The hazard-rate curves provide examples of increasing, decreasing, bathtub, and more complex non-monotonic forms.

The plots show that both skewness and kurtosis generally increase as the parameters α and c increase, while β and θ remain fixed. At lower values of α and c, the TL-MK-LLoGP distribution exhibits lower skewness and kurtosis.

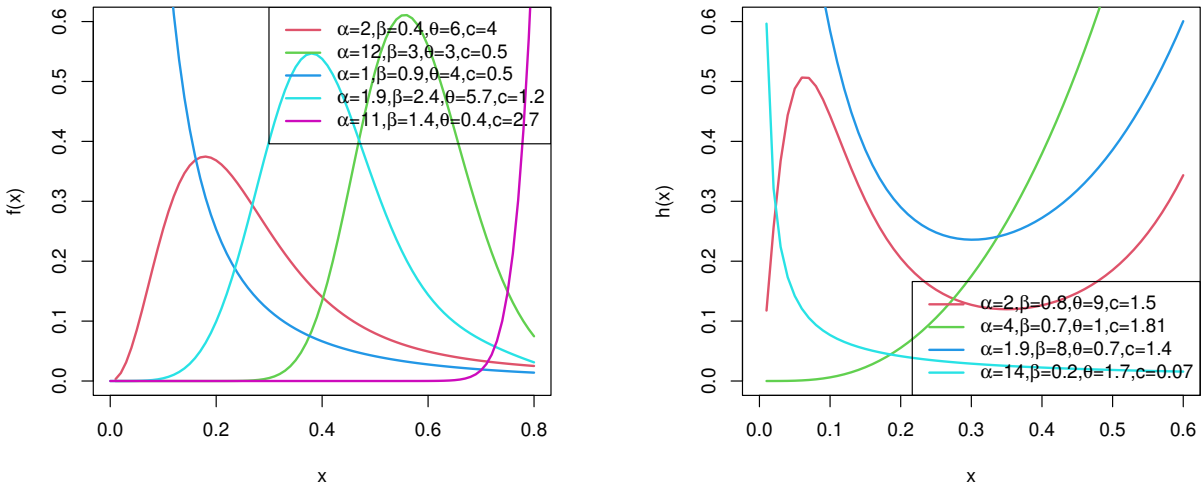


Figure 7.1. Visualization of the TL-MK-LLoGP PDF and HRF

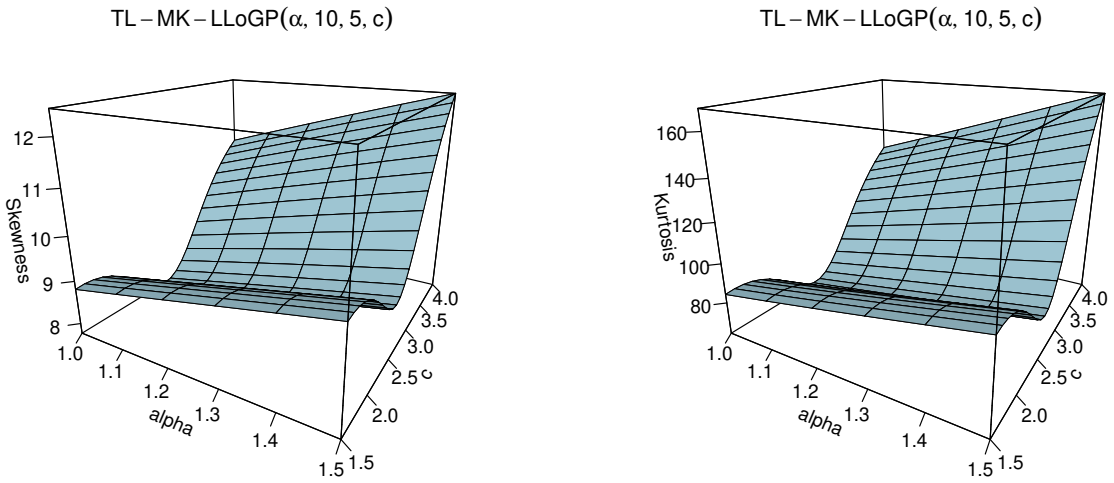


Figure 7.2. Plots of Skewness and Kurtosis for the TL-MK-LLoGP Distribution

7.2. Topp-Leone Modified Kies-Lindley Logarithmic (TL-MK-LinLog) Distribution

Let the baseline distribution be specified as the Lindley distribution with CDF and PDF given by $G(x;c) = 1 - \left(1 + \frac{cx}{c+1}\right) e^{-cx}$ and $g(x;c) = \frac{c^2}{c+1}(1+x)e^{-cx}$, respectively for $x > 0$ and $c > 0$. The CDF, PDF and HRF of the TL-MK-LinLog distribution are given by

$$F_{TL-MK-LinLog}(x;\alpha,\beta,\theta,c) = 1 - \frac{\log\left(1-\theta\left[1-\left\{1-\exp\left(-2T_L(x;\beta,c)\right)\right\}^{\alpha}\right]\right)}{\log(1-\theta)},$$

$$\begin{aligned} f_{TL-MK-LinLog}(x;\alpha,\beta,\theta,c) = {} & \frac{2\alpha\beta\theta[\frac{c^2}{c+1}(1+x)e^{-cx}][1-\left(1+\frac{cx}{c+1}\right)e^{-cx}]^{\beta-1}}{[-\log(1-\theta)][\left(1+\frac{cx}{c+1}\right)e^{-cx}]^{\beta+1}} \\ & \times \left(1-\theta\left[1-\left\{1-\exp\left(-2T_L(x;\beta,c)\right)\right\}^{\alpha}\right]\right)^{-1} \\ & \times \left\{1-\exp\left(-2T_L(x;\beta,c)\right)\right\}^{\alpha-1} \\ & \times \exp\left(-2T_L(x;\beta,c)\right), \end{aligned}$$

and

$$\begin{aligned} h_{TL-MK-LinLog}(x;\alpha,\beta,\theta,c) = {} & \frac{2\alpha\beta\theta[\frac{c^2}{c+1}(1+x)e^{-cx}][1-\left(1+\frac{cx}{c+1}\right)e^{-cx}]^{\beta-1}}{[-\log(1-\theta)][\left(1+\frac{cx}{c+1}\right)e^{-cx}]^{\beta+1}} \\ & \times \left(1-\theta\left[1-\left\{1-\exp\left(-2T_L(x;\beta,c)\right)\right\}^{\alpha}\right]\right)^{-1} \\ & \times \left\{1-\exp\left(-2T_L(x;\beta,c)\right)\right\}^{\alpha-1}\exp\left(-2T_L(x;\beta,c)\right) \\ & \times \left[\frac{\log\left(1-\theta\left[1-\left\{1-\exp\left(-2T_L(x;\beta,c)\right)\right\}^{\alpha}\right]\right)}{\log(1-\theta)}\right]^{-1}, \end{aligned}$$

respectively, for $x,\alpha,\beta,\theta,c>0$, where

$$T_L(x;\beta,c) = \left(\frac{1-\left(1+\frac{cx}{c+1}\right)e^{-cx}}{\left(1+\frac{cx}{c+1}\right)e^{-cx}}\right)^{\beta}.$$

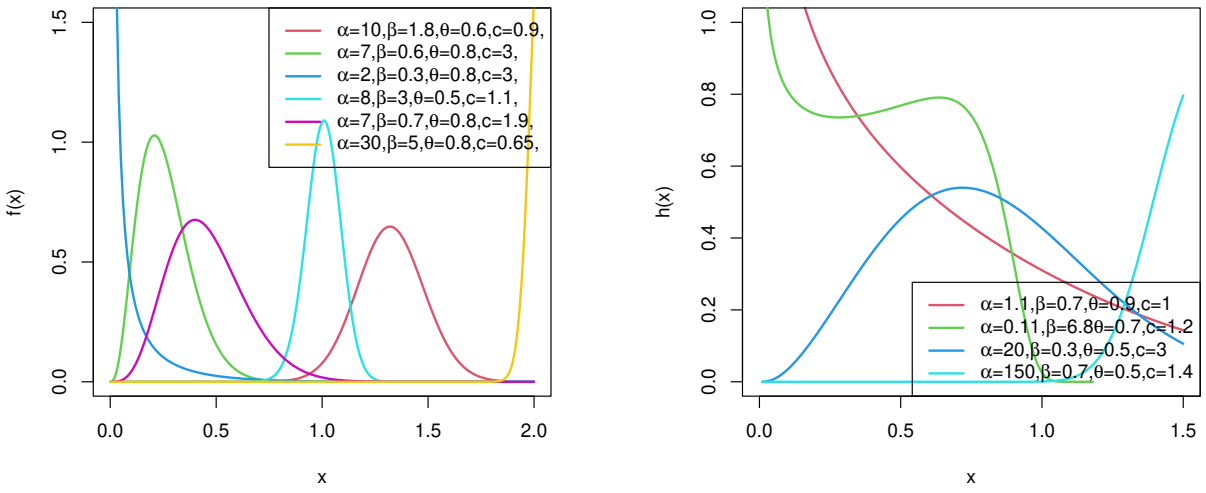


Figure 7.3. Visualization of the TL-MK-LinLog PDF and HRF

The plots of PDF and HRF for the TL-MK-LinLog distribution are shown in Figure 7.3. The PDF exhibit unimodal, reverse-J, J-shaped, almost symmetric, right and left-skewed shapes. The hazard rate function exhibits both monotonic and non-monotonic shapes, including increasing, decreasing, upside-down shape and bathtub followed by upside-down bathtub.

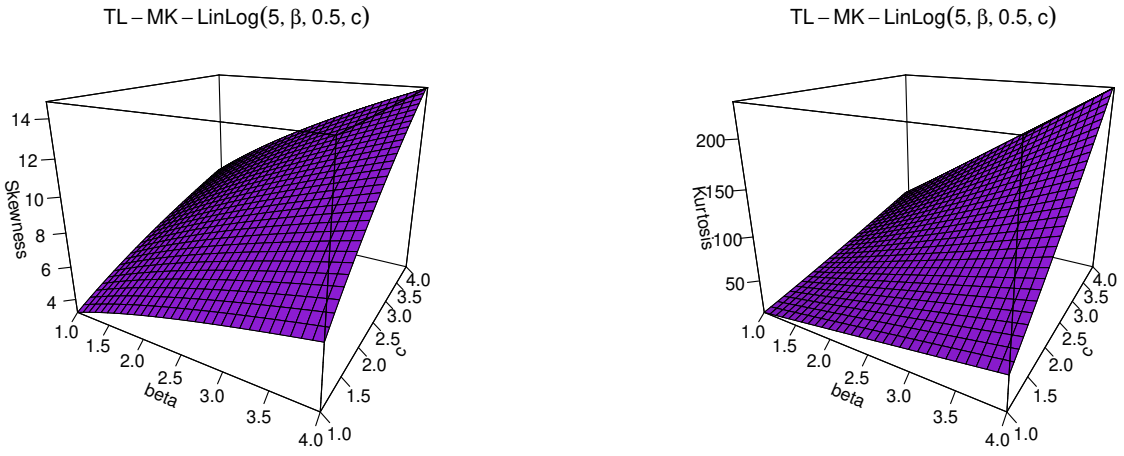


Figure 7.4. Plots of Skewness and Kurtosis for the TL-MK-LinLog Distribution

According to figure 7.4, the plots show that both skewness and kurtosis increase as the parameters β and c increase, while α and θ remain fixed. Lower values of β and c are associated with smaller skewness and kurtosis values.

7.3. Topp-Leone Modified Kies-Uniform Geometric (TL-MK-UG) Distribution

The uniform distribution is considered with CDF and PDF given by $G(x;b) = \frac{x}{b}$ and $g(x;b) = \frac{1}{b}$ respectively for $b > 0$ and $0 < x < b$ as the baseline distribution. The CDF, PDF and HRF of the TL-MK-UG distribution are given by

$$F_{TL-MK-UG}(x;\alpha,\beta,\theta,b) = 1 - \frac{(1-\theta)\left[1-\left\{1-\exp\left(-2\left(\frac{\frac{x}{b}}{1-\frac{x}{b}}\right)^{\beta}\right)\right\}^{\alpha}\right]}{(1-\theta\left[1-\{1-\exp\left(-2T_U(x;\beta,b)\right)\}^{\alpha}\right])},$$

$$\begin{aligned} f_{TL-MK-UG}(x;\alpha,\beta,\theta,b) = {} & \frac{2\alpha\beta\theta[\frac{1}{b}][\frac{x}{b}]^{\beta-1}}{\theta(1-\theta)^{-1}[1-\frac{x}{b}]^{\beta+1}}\exp\left(-2T_U(x;\beta,b)\right) \\ & \times\{1-\exp\left(-2T_U(x;\beta,b)\right)\}^{\alpha-1} \\ & \times\left(1-\theta\left[1-\{1-\exp\left(-2T_U(x;\beta,b)\right)\}^{\alpha}\right]\right)^{-2}, \end{aligned}$$

and

$$
\begin{aligned}
h_{TL-MK-UG}(x;\alpha,\beta,\theta,b) = & \frac{2\alpha\beta\theta[\frac{1}{b}][\frac{x}{b}]^{\beta-1}\left(1-\theta\left[1-\{1-\exp\left(-2T_U(x;\beta,b)\right)\}^{\alpha}\right]\right)^{-2}}{[1-\frac{x}{b}]^{\beta+1}\left(\theta(1-\theta)^{-1}\right)} \\
& \times \{1-\exp\left(-2T_U(x;\beta,b)\right)\}^{\alpha-1} \\
& \times \exp\left(-2T_U(x;\beta,b)\right) \\
& \times \left\{\frac{(1-\theta)\left[1-\left\{1-\exp\left(-2\left(\frac{\frac{x}{b}}{1-\frac{x}{b}}\right)^{\beta}\right)\right\}^{\alpha}\right]}{\left(1-\theta\left[1-\{1-\exp\left(-2T_U(x;\beta,b)\right)\}^{\alpha}\right]\right)}\right\}^{-1}
\end{aligned} \tag{7.1}
$$

respectively, for $\alpha,\beta,\theta,b>0$, where $T_U(x;\beta,b)=\left(\frac{\frac{x}{b}}{1-\frac{x}{b}}\right)^{\beta}$.

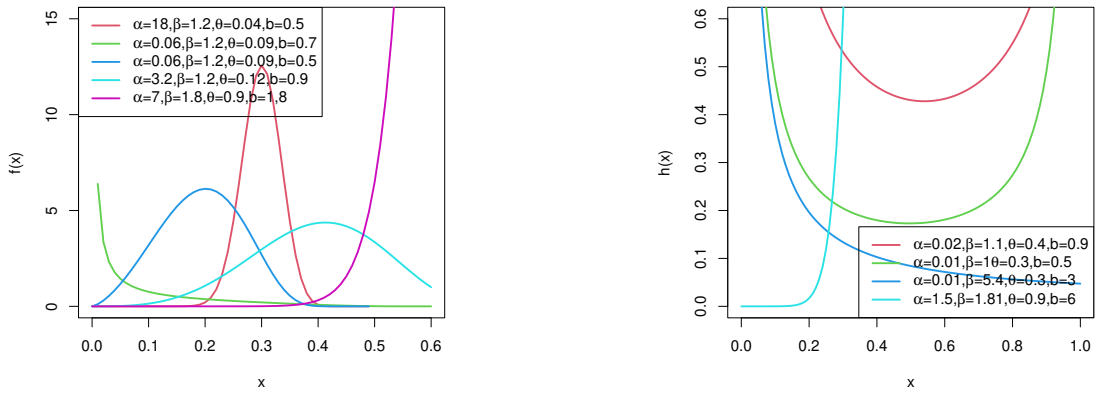


Figure 7.5. Visualization of the TL-MK-UG PDF and HRF

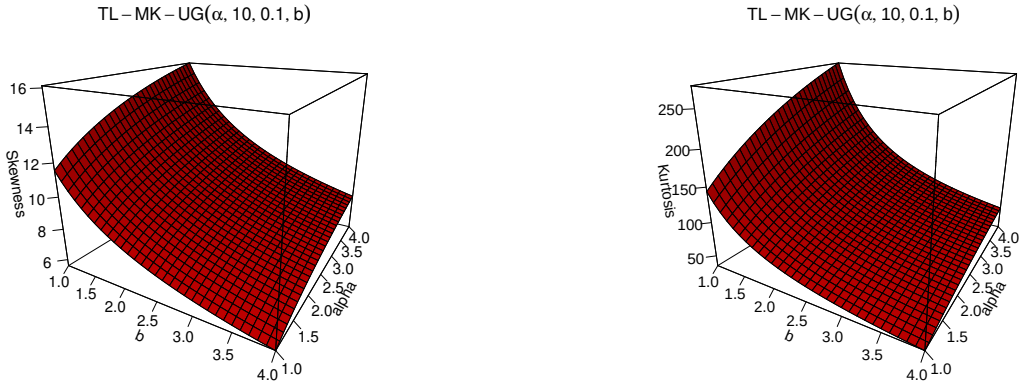


Figure 7.6. Plots of Skewness and Kurtosis for the TL-MK-UG Distribution

Figure 7.5 presents the plots of PDF and HRF for the TL-MK-UG distribution. The PDF can capture unimodal, reverse-J, J-shaped, almost symmetric, right and left-skewed shapes. The hazard rate function plot displays both monotonic and non-monotonic shapes.

Figure 7.6 show that both skewness and kurtosis decrease as the parameters α and b increase, while β and θ remain fixed. Higher skewness and kurtosis values occur at lower values of α and b.

8. Monte Carlo Simulations

A Monte Carlo simulation study was conducted to assess the reliability of the estimation methods under consideration for the parameters of the TL-MK-LLoGP distribution. We simulate $N = 3000$ independent samples from the TL-MK-LLoGP distribution, with sample sizes of $n = 25, 50, 100, 200, 400,$ and 800 to assess the efficiency of the different estimation methods. We used the metrics: average bias (ABias) and root mean square error (RMSE). The ABias and RMSE for the estimated parameter, say, $\hat{\alpha}$, are given by

$$ABias(\hat{\alpha}) = \frac{1}{N}\sum_{i=1}^{N}(\hat{\alpha}_i - \alpha), \quad \text{and} \quad RMSE(\hat{\alpha}) = \sqrt{\frac{\sum_{i=1}^{N}(\hat{\alpha}_i - \alpha)^2}{N}},$$

respectively. The row indicating $\sum ranks$ represents the partial sum of the ranks. Among all the estimators for a given metric, the superscript indicates their rank.

Table 8.1. Simulation Results for Different Estimation Methods for $\alpha = 1.3, \beta = 2.5, \theta = 0.2, c = 0.8$

		ML		LS		WLS		CVM		AD	
n	Parameter	ABIAS	RMSE	ABIAS	RMSE	ABIAS	RMSE	ABIAS	RMSE	ABIAS	RMSE
25	α	$0.2633^{\{1\}}$	$0.5110^{\{1\}}$	$2.4630^{\{5\}}$	$2.9531^{\{5\}}$	$2.4495^{\{4\}}$	$2.8040^{\{4\}}$	$2.3164^{\{3\}}$	$2.5168^{\{3\}}$	$2.0869^{\{2\}}$	$2.2761^{\{2\}}$
	β	$0.0749^{\{1\}}$	$0.1787^{\{1\}}$	$0.5146^{\{4\}}$	$0.9767^{\{2\}}$	$0.4031^{\{3\}}$	$0.9768^{\{3\}}$	$0.6215^{\{5\}}$	$0.9811^{\{4\}}$	$0.0956^{\{2\}}$	$1.6335^{\{5\}}$
	θ	$0.5345^{\{3\}}$	$0.7438^{\{2\}}$	$0.2804^{\{1\}}$	$0.5921^{\{1\}}$	$1.2401^{\{5\}}$	$2.5939^{\{5\}}$	$0.3131^{\{2\}}$	$0.8168^{\{3\}}$	$0.7116^{\{4\}}$	$1.7055^{\{4\}}$
	c	$0.0136^{\{1\}}$	$0.0983^{\{1\}}$	$0.5199^{\{4\}}$	$0.8127^{\{5\}}$	$0.5620^{\{5\}}$	$0.7925^{\{4\}}$	$0.1569^{\{2\}}$	$0.3159^{\{2\}}$	$0.1930^{\{3\}}$	$0.4262^{\{3\}}$
	$\sum$ ranks	11		27		33		24		25	
50	α	$0.1668^{\{1\}}$	$0.3333^{\{1\}}$	$2.1575^{\{4\}}$	$2.8724^{\{5\}}$	$2.2455^{\{5\}}$	$2.7483^{\{4\}}$	$2.2495^{\{3\}}$	$2.3187^{\{3\}}$	$1.7547^{\{2\}}$	$1.9566^{\{2\}}$
	β	$0.0490^{\{1\}}$	$0.1206^{\{1\}}$	$0.4173^{\{4\}}$	$0.6390^{\{3\}}$	$0.3823^{\{2\}}$	$0.5229^{\{2\}}$	$0.4572^{\{5\}}$	$0.6698^{\{4\}}$	$0.0879^{\{1\}}$	$0.7024^{\{5\}}$
	θ	$0.3352^{\{3\}}$	$0.5034^{\{1\}}$	$0.1333^{\{1\}}$	$0.5078^{\{2\}}$	$1.1311^{\{5\}}$	$2.2294^{\{5\}}$	$0.2189^{\{2\}}$	$0.6359^{\{3\}}$	$0.6916^{\{4\}}$	$1.5217^{\{4\}}$
	c	$0.0053^{\{1\}}$	$0.0714^{\{1\}}$	$0.3449^{\{3\}}$	$0.7181^{\{5\}}$	$0.4465^{\{5\}}$	$0.5340^{\{4\}}$	$0.0759^{\{2\}}$	$0.2480^{\{2\}}$	$0.0825^{\{4\}}$	$0.1409^{\{3\}}$
	$\sum$ ranks	10		27		32		24		26	
100	α	$0.1037^{\{1\}}$	$0.2051^{\{1\}}$	$1.8484^{\{3\}}$	$1.9523^{\{3\}}$	$2.0487^{\{4\}}$	$2.5142^{\{5\}}$	$2.0897^{\{5\}}$	$2.1832^{\{4\}}$	$1.4894^{\{2\}}$	$1.6108^{\{2\}}$
	β	$0.0313^{\{1\}}$	$0.0727^{\{1\}}$	$0.3999^{\{4\}}$	$0.4682^{\{3\}}$	$0.1045^{\{2\}}$	$0.3798^{\{2\}}$	$0.4297^{\{5\}}$	$0.4955^{\{5\}}$	$0.0366^{\{1\}}$	$0.4719^{\{4\}}$
	θ	$0.2013^{\{3\}}$	$0.3320^{\{2\}}$	$0.0933^{\{2\}}$	$0.3626^{\{3\}}$	$1.0657^{\{5\}}$	$2.0575^{\{5\}}$	$0.0845^{\{1\}}$	$0.3219^{\{1\}}$	$0.6287^{\{4\}}$	$1.3769^{\{4\}}$
	c	$0.0025^{\{1\}}$	$0.0463^{\{1\}}$	$0.2022^{\{3\}}$	$0.4164^{\{4\}}$	$0.2968^{\{5\}}$	$0.5290^{\{5\}}$	$0.0357^{\{2\}}$	$0.2438^{\{2\}}$	$0.0583^{\{4\}}$	$0.1276^{\{3\}}$
	$\sum$ ranks	11		25		33		25		24	
200	α	$0.0559^{\{1\}}$	$0.1412^{\{1\}}$	$0.9007^{\{2\}}$	$0.9491^{\{2\}}$	$1.7469^{\{4\}}$	$1.7762^{\{4\}}$	$2.0039^{\{5\}}$	$2.0562^{\{5\}}$	$1.4487^{\{3\}}$	$1.5668^{\{3\}}$
	β	$0.0169^{\{1\}}$	$0.0477^{\{1\}}$	$0.3918^{\{4\}}$	$0.4134^{\{4\}}$	$0.0783^{\{2\}}$	$0.1495^{\{2\}}$	$0.4096^{\{5\}}$	$0.4300^{\{5\}}$	$0.0110^{\{1\}}$	$0.4083^{\{3\}}$
	θ	$0.1226^{\{3\}}$	$0.2346^{\{2\}}$	$0.0636^{\{2\}}$	$0.2537^{\{3\}}$	$0.4820^{\{4\}}$	$0.8746^{\{5\}}$	$0.0522^{\{1\}}$	$0.1399^{\{1\}}$	$0.5168^{\{5\}}$	$0.5498^{\{4\}}$
	c	$0.0012^{\{1\}}$	$0.0332^{\{1\}}$	$0.1436^{\{4\}}$	$0.2158^{\{3\}}$	$0.1367^{\{3\}}$	$0.2809^{\{5\}}$	$0.0173^{\{2\}}$	$0.1079^{\{2\}}$	$0.0284^{\{5\}}$	$0.1136^{\{4\}}$
	$\sum$ ranks	14		24		31		26		28	
400	α	$0.0273^{\{1\}}$	$0.0940^{\{1\}}$	$0.8125^{\{2\}}$	$0.8344^{\{2\}}$	$0.8783^{\{3\}}$	$0.8924^{\{3\}}$	$1.8584^{\{5\}}$	$1.8827^{\{5\}}$	$0.7047^{\{1\}}$	$0.9446^{\{4\}}$
	β	$0.0081^{\{1\}}$	$0.0291^{\{1\}}$	$0.4006^{\{4\}}$	$0.4088^{\{4\}}$	$0.0489^{\{2\}}$	$0.0847^{\{2\}}$	$0.4046^{\{5\}}$	$0.4124^{\{5\}}$	$0.0013^{\{1\}}$	$0.1368^{\{3\}}$
	θ	$0.0579^{\{3\}}$	$0.1593^{\{2\}}$	$0.0242^{\{1\}}$	$0.1290^{\{1\}}$	$0.2036^{\{4\}}$	$0.7884^{\{5\}}$	$0.0475^{\{2\}}$	$0.1114^{\{2\}}$	$0.3031^{\{5\}}$	$0.4722^{\{4\}}$
	c	$0.0005^{\{2\}}$	$0.0248^{\{1\}}$	$0.0949^{\{4\}}$	$0.1412^{\{4\}}$	$0.0667^{\{3\}}$	$0.2180^{\{5\}}$	$0.0107^{\{1\}}$	$0.0923^{\{2\}}$	$0.0245^{\{5\}}$	$0.0872^{\{3\}}$
	$\sum$ ranks	12		22		27		30		26	
800	α	$0.0139^{\{2\}}$	$0.0704^{\{1\}}$	$0.5428^{\{4\}}$	$0.6339^{\{4\}}$	$0.1626^{\{3\}}$	$0.1692^{\{2\}}$	$0.8538^{\{5\}}$	$0.8648^{\{5\}}$	$0.3850^{\{1\}}$	$0.3970^{\{3\}}$
	β	$0.0046^{\{2\}}$	$0.0192^{\{1\}}$	$0.1056^{\{4\}}$	$0.3094^{\{4\}}$	$0.0340^{\{3\}}$	$0.0403^{\{2\}}$	$0.4015^{\{5\}}$	$0.4105^{\{5\}}$	$0.0010^{\{1\}}$	$0.0608^{\{3\}}$
	θ	$0.0266^{\{2\}}$	$0.1190^{\{2\}}$	$0.0181^{\{1\}}$	$0.0970^{\{1\}}$	$0.1584^{\{4\}}$	$0.4317^{\{5\}}$	$0.0259^{\{3\}}$	$0.0856^{\{2\}}$	$0.2951^{\{5\}}$	$0.3638^{\{4\}}$
	c	$0.0001^{\{1\}}$	$0.0188^{\{1\}}$	$0.0846^{\{4\}}$	$0.1366^{\{4\}}$	$0.0480^{\{3\}}$	$0.0979^{\{3\}}$	$0.0065^{\{2\}}$	$0.0802^{\{2\}}$	$0.0164^{\{5\}}$	$0.0595^{\{2\}}$
	$\sum$ ranks	14		26		29		31		29	

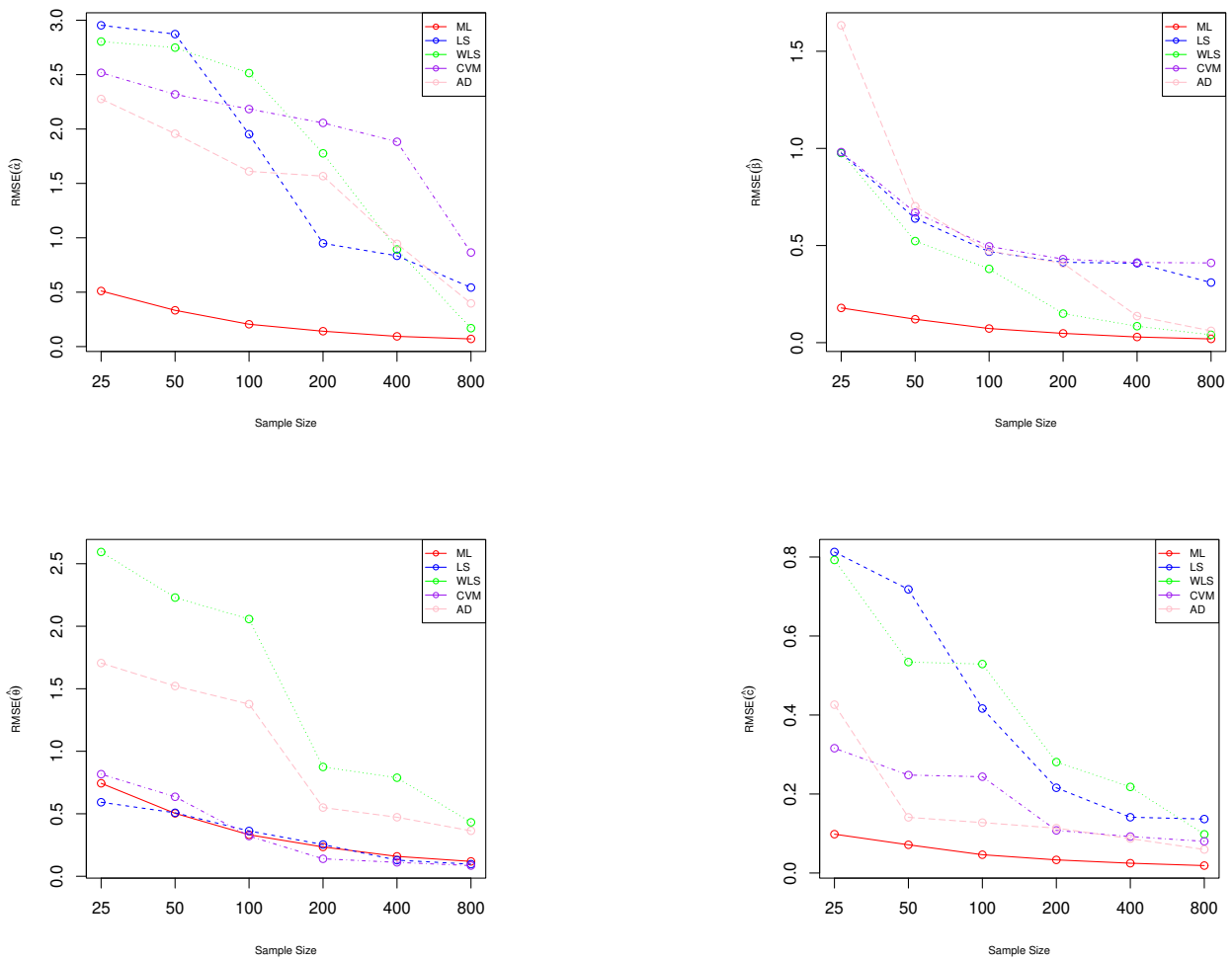


Figure 8.1. RMSE Plots for Table 8.1

Table 8.2. Simulation Results for Different Estimation Methods for $\alpha = 0.8, \beta = 0.8, \theta = 1.3, c = 0.7$

		ML		LS		WLS		CVM		AD	
n	Parameter	ABIAS	RMSE	ABIAS	RMSE	ABIAS	RMSE	ABIAS	RMSE	ABIAS	RMSE
25	α	$0.0275^{\{1\}}$	$0.1157^{\{1\}}$	$1.0967^{\{3\}}$	$1.1408^{\{2\}}$	$0.5449^{\{2\}}$	$0.5783^{\{2\}}$	$1.5729^{\{5\}}$	$1.6292^{\{3\}}$	$1.4773^{\{4\}}$	$1.7008^{\{4\}}$
	β	$0.0541^{\{1\}}$	$0.2107^{\{1\}}$	$1.7201^{\{4\}}$	$1.7373^{\{3\}}$	$1.5384^{\{2\}}$	$1.5589^{\{2\}}$	$1.6949^{\{3\}}$	$1.7209^{\{3\}}$	$3.4307^{\{5\}}$	$3.7185^{\{5\}}$
	θ	$0.0574^{\{1\}}$	$0.4895^{\{1\}}$	$1.0385^{\{4\}}$	$1.9490^{\{4\}}$	$0.9991^{\{3\}}$	$1.9934^{\{5\}}$	$0.2272^{\{2\}}$	$1.1289^{\{2\}}$	$0.4823^{\{5\}}$	$2.1449^{\{6\}}$
	c	$0.0441^{\{1\}}$	$0.1536^{\{1\}}$	$0.3722^{\{4\}}$	$0.5104^{\{3\}}$	$0.2907^{\{3\}}$	$0.9289^{\{6\}}$	$0.8261^{\{5\}}$	$0.8615^{\{5\}}$	$0.1009^{\{2\}}$	$0.4338^{\{2\}}$
	$\sum$ ranks	8		25		23		28		33	
50	α	$0.0212^{\{1\}}$	$0.0877^{\{1\}}$	$1.0325^{\{2\}}$	$1.0525^{\{2\}}$	$0.4545^{\{1\}}$	$0.4708^{\{1\}}$	$1.4879^{\{5\}}$	$1.5125^{\{3\}}$	$0.9996^{\{3\}}$	$0.9566^{\{2\}}$
	β	$0.0355^{\{1\}}$	$0.1316^{\{1\}}$	$1.5920^{\{5\}}$	$1.6437^{\{4\}}$	$1.4902^{\{3\}}$	$1.4979^{\{2\}}$	$1.3356^{\{1\}}$	$1.3928^{\{1\}}$	$1.5148^{\{4\}}$	$2.7735^{\{5\}}$
	θ	$0.0203^{\{1\}}$	$0.3301^{\{1\}}$	$1.0216^{\{5\}}$	$1.0475^{\{2\}}$	$0.4638^{\{3\}}$	$1.1118^{\{4\}}$	$0.0985^{\{2\}}$	$0.7055^{\{3\}}$	$0.3041^{\{4\}}$	$2.0315^{\{5\}}$
	c	$0.0330^{\{1\}}$	$0.1148^{\{1\}}$	$0.3207^{\{4\}}$	$0.5021^{\{4\}}$	$0.0940^{\{2\}}$	$0.4896^{\{3\}}$	$0.7857^{\{5\}}$	$0.8047^{\{5\}}$	$0.0825^{\{1\}}$	$0.3717^{\{2\}}$
	$\sum$ ranks	8		28		19		25		31	
100	α	$0.0108^{\{1\}}$	$0.0582^{\{1\}}$	$0.3120^{\{2\}}$	$0.3231^{\{2\}}$	$0.2280^{\{1\}}$	$0.2361^{\{1\}}$	$1.3644^{\{5\}}$	$1.3756^{\{4\}}$	$0.6385^{\{3\}}$	$0.6629^{\{3\}}$
	β	$0.0149^{\{1\}}$	$0.0816^{\{1\}}$	$1.2168^{\{3\}}$	$1.4565^{\{4\}}$	$1.4452^{\{5\}}$	$1.4484^{\{3\}}$	$1.0629^{\{2\}}$	$1.2277^{\{2\}}$	$0.0344^{\{1\}}$	$1.7330^{\{5\}}$
	θ	$0.0108^{\{1\}}$	$0.2090^{\{1\}}$	$0.5929^{\{4\}}$	$0.7078^{\{3\}}$	$0.4174^{\{3\}}$	$0.8331^{\{4\}}$	$0.0828^{\{1\}}$	$0.5958^{\{2\}}$	$0.3004^{\{2\}}$	$1.0079^{\{5\}}$
	c	$0.0165^{\{1\}}$	$0.0745^{\{1\}}$	$0.2432^{\{3\}}$	$0.4168^{\{4\}}$	$0.0612^{\{1\}}$	$0.2611^{\{2\}}$	$0.4517^{\{5\}}$	$0.5275^{\{5\}}$	$0.0756^{\{2\}}$	$0.1978^{\{1\}}$
	$\sum$ ranks	8		25		20		26		22	
200	α	$0.0079^{\{1\}}$	$0.0421^{\{1\}}$	$0.2393^{\{2\}}$	$0.3177^{\{3\}}$	$0.0934^{\{1\}}$	$0.1383^{\{2\}}$	$0.7613^{\{5\}}$	$0.8333^{\{5\}}$	$0.4466^{\{4\}}$	$0.5630^{\{4\}}$
	β	$0.0117^{\{1\}}$	$0.0589^{\{1\}}$	$0.7852^{\{3\}}$	$0.7864^{\{2\}}$	$1.3973^{\{5\}}$	$1.3990^{\{5\}}$	$0.7805^{\{2\}}$	$0.7817^{\{1\}}$	$0.0143^{\{1\}}$	$1.2718^{\{4\}}$
	θ	$0.0059^{\{1\}}$	$0.1304^{\{1\}}$	$0.3976^{\{4\}}$	$0.4309^{\{3\}}$	$0.2989^{\{3\}}$	$0.1371^{\{2\}}$	$0.0676^{\{2\}}$	$0.3336^{\{4\}}$	$0.1302^{\{5\}}$	$0.4897^{\{5\}}$
	c	$0.0121^{\{1\}}$	$0.0532^{\{1\}}$	$0.1840^{\{4\}}$	$0.3947^{\{5\}}$	$0.0299^{\{2\}}$	$0.2188^{\{3\}}$	$0.2905^{\{5\}}$	$0.3600^{\{4\}}$	$0.0396^{\{3\}}$	$0.0580^{\{2\}}$
	$\sum$ ranks	8		26		28		28		28	
400	α	$0.0032^{\{1\}}$	$0.0294^{\{1\}}$	$0.1950^{\{3\}}$	$0.2976^{\{3\}}$	$0.0539^{\{1\}}$	$0.1053^{\{1\}}$	$0.3377^{\{5\}}$	$0.3403^{\{4\}}$	$0.3129^{\{4\}}$	$0.4116^{\{5\}}$
	β	$0.0045^{\{1\}}$	$0.0405^{\{1\}}$	$0.5788^{\{3\}}$	$0.6189^{\{3\}}$	$1.3565^{\{5\}}$	$1.3574^{\{5\}}$	$0.4313^{\{2\}}$	$0.5374^{\{2\}}$	$0.0106^{\{1\}}$	$0.9740^{\{4\}}$
	θ	$0.0028^{\{1\}}$	$0.0753^{\{1\}}$	$0.1093^{\{3\}}$	$0.2443^{\{3\}}$	$0.0969^{\{2\}}$	$0.1097^{\{2\}}$	$0.0382^{\{1\}}$	$0.2579^{\{4\}}$	$0.0290^{\{1\}}$	$0.3469^{\{5\}}$
	c	$0.0051^{\{1\}}$	$0.0373^{\{1\}}$	$0.0583^{\{3\}}$	$0.2819^{\{5\}}$	$0.0173^{\{1\}}$	$0.1946^{\{3\}}$	$0.1452^{\{5\}}$	$0.2805^{\{4\}}$	$0.0309^{\{2\}}$	$0.0523^{\{2\}}$
	$\sum$ ranks	8		26		22		27		25	
800	α	$0.0019^{\{1\}}$	$0.0217^{\{1\}}$	$0.1010^{\{3\}}$	$0.1022^{\{2\}}$	$0.0274^{\{2\}}$	$0.0683^{\{1\}}$	$0.3246^{\{5\}}$	$0.3259^{\{4\}}$	$0.2583^{\{4\}}$	$0.2750^{\{3\}}$
	β	$0.0019^{\{1\}}$	$0.0294^{\{1\}}$	$0.4768^{\{3\}}$	$0.5879^{\{3\}}$	$1.3170^{\{5\}}$	$1.3174^{\{5\}}$	$0.1788^{\{2\}}$	$0.3882^{\{2\}}$	$0.0011^{\{1\}}$	$0.8724^{\{4\}}$
	θ	$0.0012^{\{1\}}$	$0.0491^{\{1\}}$	$0.0930^{\{3\}}$	$0.1455^{\{3\}}$	$0.0506^{\{2\}}$	$0.0657^{\{1\}}$	$0.0324^{\{1\}}$	$0.0993^{\{2\}}$	$0.0064^{\{1\}}$	$0.1302^{\{4\}}$
	c	$0.0032^{\{1\}}$	$0.0276^{\{1\}}$	$0.0216^{\{3\}}$	$0.1108^{\{4\}}$	$0.0171^{\{2\}}$	$0.0976^{\{3\}}$	$0.1052^{\{5\}}$	$0.1484^{\{5\}}$	$0.0267^{\{4\}}$	$0.0312^{\{2\}}$
	$\sum$ ranks	8		24		23		26		28	

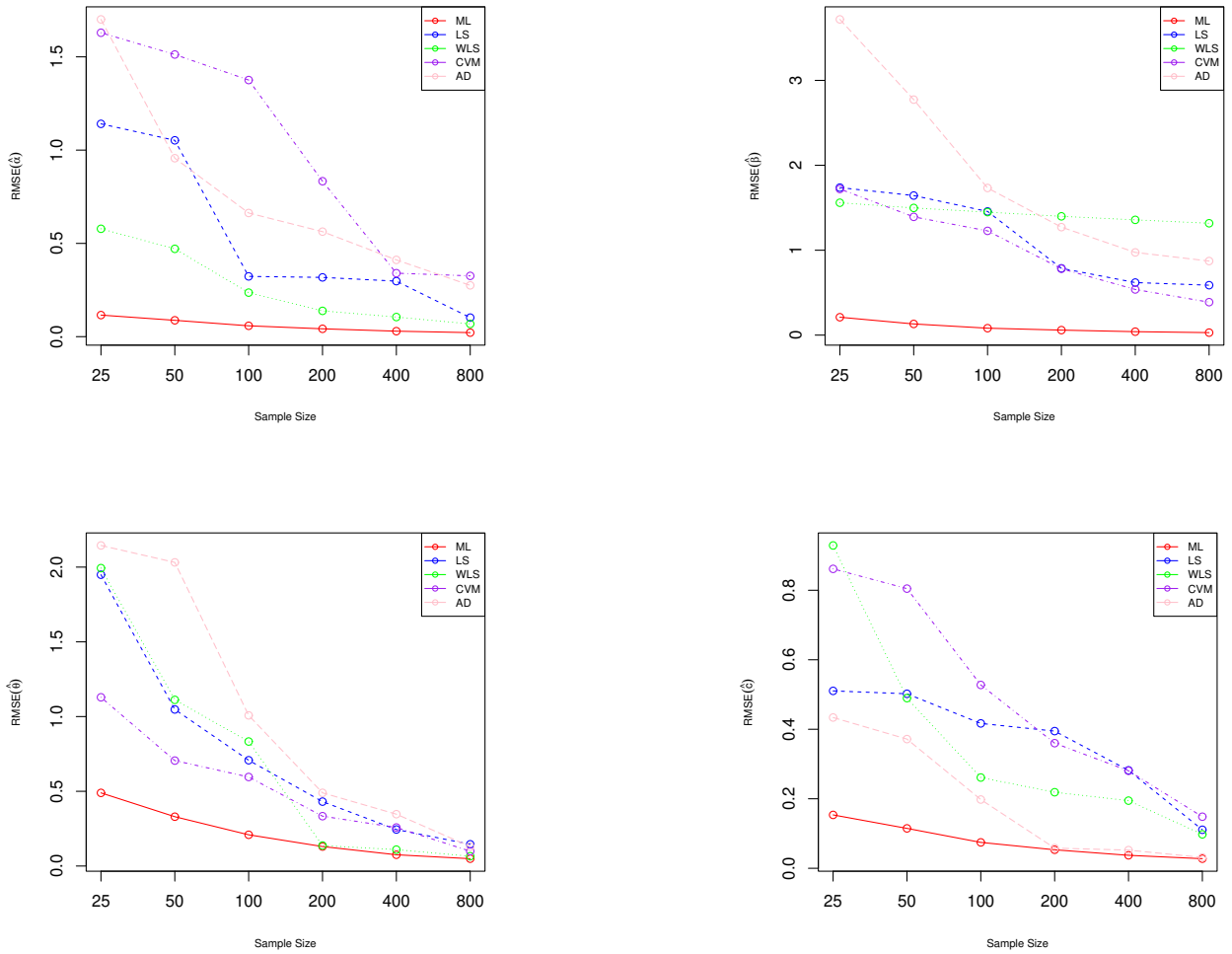


Figure 8.2. RMSE Plots for Table 8.2

Table 8.3. Partial and Overall Ranks of all Estimation Methods

Parameters	n	ML	WLS	LS	AD	CVM
$\alpha = 1.3, \beta = 2.5, \theta = 0.2, c = 0.8$	25	1	5	4	3	2
	50	1	5	4	3	2
	100	1	5	3.5	2	3.5
	200	1	5	2	4	3
	400	1	4	2	3	5
	800	1	3.5	2	3.5	5
$\alpha = 0.8, \beta = 0.8, \theta = 1.3, c = 0.7$	25	1	2	3	5	4
	50	1	2	4	5	3
	100	1	2	4	3	5
	200	1	4	2	4	4
	400	1	2	4	3	5
	800	1	2	3	5	4
$\sum$ ranks		12	41.5	37.5	43.5	45.5
Overall rank		1	3	2	4	5

Tables 8.1 and 8.2 report the simulation results for the estimation methods considered. In each row, the superscript attached to the ABIAS and RMSE values represents the rank of the corresponding method, where rank 1 indicates the smallest value. The row labelled $\sum$ ranks gives the partial sum of ranks for each estimation method at a given sample size.

The simulation results provide qualified evidence concerning estimation reliability. For the two parameter settings considered, the average bias and RMSE of the maximum likelihood estimates generally decreased as the sample size increased. This indicates improved finite-sample accuracy for the four-parameter TL-MK-LLoGP model under the investigated settings. However, the comparatively large bias and RMSE produced by some alternative estimators, particularly for smaller samples, show that the additional parameters can make estimation sensitive to the estimation method and sample size. These simulations do not rule out weak identification, parameter correlation, or numerical instability near parameter boundaries. In applications, estimation should therefore be supported by multiple starting values, convergence checks, profile-likelihood plots, and comparison with parsimonious submodels.

Table 8.3 presents the partial and overall ranks of the estimation methods across the two parameter settings. The results show that the ABIAS and RMSE values generally decrease as the sample size increases, suggesting that the estimators become more accurate and stable for larger samples. Overall, the ML method performs best, followed by LS and WLS, while CVM records the highest overall rank.

The comparatively large bias and RMSE observed for LS, WLS, CVM, and AD are concentrated mainly in the shape parameters and are more pronounced for smaller sample sizes and some parameter settings. These methods estimate the parameters by minimizing discrepancies between the theoretical and empirical distribution functions. In the four-parameter TL-MK-LLoGP model, different parameter combinations may produce similar CDF shapes, making the individual parameters more difficult to recover accurately through these distance-based criteria. The weighting schemes used by WLS and AD can also make their finite-sample performance sensitive to observations in particular regions of the distribution. The results do not indicate failure to obtain numerical solutions, but show that convergence does not necessarily ensure accurate parameter recovery. Although these methods remain useful as alternative estimation procedures and sensitivity checks, the simulation results support ML as the preferred method for the parameter settings examined. This conclusion is limited to the TL-MK-LLoGP model and simulation settings considered here.

Figures 8.1 and 8.2 display the RMSE plots for the four parameters. The plots further confirm that RMSE values decline as the sample size increases for the estimation methods. **Other simulation studies using the TL-MK-LinLog and TL-MK-UG distributions are reported in the appendix.**

9. Risk Measures

This section outlines a range of risk measures frequently used in finance and actuarial science to evaluate potential portfolio risks. These include value at risk (VaR), tail value at risk (TVaR), tail variance (TV), and tail variance premium (TVP).

9.1. Value at Risk

Value at Risk (VaR) is a widely used risk measure in actuarial science for evaluating financial market risk. Also known as the quantile risk measure or the quantile premium principle, VaR is typically defined at a specific confidence level, such as 90%, 95%, or 99%. The VaR for TL-MK-GPS class of distributions is

$$VaR_p = G^{-1}\left(\frac{\left\{-\frac{1}{2}\left\{\ln\left[1-\{1-\theta^{-1}C^{-1}[(1-p)C(\theta)]\}^{\frac{1}{\alpha}}\right]\right\}\right\}^{\frac{1}{\beta}}}{1+\left[\left\{-\frac{1}{2}\left\{\ln\left[1-\{1-\theta^{-1}C^{-1}[(1-p)C(\theta)]\}^{\frac{1}{\alpha}}\right]\right\}\right\}^{\frac{1}{\beta}}\right]}\right),$$

where $0 < p < 1$ is a specified level of significance.

9.2. Tail Value at Risk

Tail Value at Risk (TVaR) is another important metric in actuarial science that estimates the expected loss given that the loss exceeds a specified probability threshold. It is also known as Conditional Tail Expectation (CTE) or Tail Conditional Expectation (TCE). For the TL-MK-GPS class of distributions, the TVaR is expressed as

$$\begin{aligned} TVaR_p &= E(X|X > x_p) \\ &= \frac{1}{1-p}\int_{VaR_p}^{\infty} x f(x)\,dx \\ &= \frac{1}{1-p}\sum_{i=0}^{\infty}\int_{VaR_p}^{\infty} x\delta_{i+1}h_{i+1}(x;\psi)\,dx, \end{aligned}$$

where δ_{i+1} is defined by Equation (3.3) and $h_{i+1}(x;\psi)$ is the Exp-G density with power parameter $(i+1)$.

9.3. Tail Variance

Tail Variance (TV) is a fundamental actuarial measure that quantifies the variability of losses beyond the value at risk (VaR) threshold. For the TL-MK-GPS distribution class, TV is expressed as follows:

$$\begin{aligned} TV_p &= E(X^2|X > x_p) - (TVaR_p)^2 \\ &= \frac{1}{1-p}\int_{VaR_p}^{\infty} x^2 f(x)\,dx - (TVaR_p)^2 \\ &= \frac{1}{1-p}\sum_{i=0}^{\infty}\delta_{i+1}\int_{VaR_p}^{\infty} x^2 h_{i+1}(x;\psi)\,dx - (TVaR_p)^2, \end{aligned}$$

where δ_{i+1} is defined by Equation (3.3) and $h_{i+1}(x;\psi)$ is the Exp-G density with power parameter $(i+1)$.

9.4. Tail Variance Premium

Tail Variance Premium (TVP) is an important actuarial indicator, particularly relevant in insurance analysis. For the TL-MK-GPS class of distributions the TVP is

$$TVP_p = TVaR_p + \nu(TV_p),$$

where $0 < \nu < 1$.

In the simulation study and numerical applications, the value of ν was taken to be equal to the confidence level p used in the calculation of the risk measures.

9.5. Numerical Study for the Risk Measures

In this subsection, we conduct a numerical simulation study of the risk measures; VaR, TVaR, TV, and TVP for the Topp-Leone-modified Kies log-logistic Poisson distribution. The results are compared with those of its sub-model: TL-MK-LLoGP($\alpha = 1$) as well as with the non-nested Alpha Power Weibull (APW) distribution by Nassar et al. (2017) and the Alpha Power Topp–Leone Weibull (APTLW) distribution by Benkhelifa (2022).

The simulation procedure was carried out as follows:

1. For each distribution, random samples of size $n = 100$ were generated, and parameters were estimated via the method of maximum likelihood.
2. Each simulation was repeated 3000 times to compute the corresponding values of VaR, TVaR, TV, and TVP.

Table 9.1 presents the numerical results for the four risk measures across the compared distributions. In practical terms, a higher VaR indicates a larger loss threshold at the specified confidence level, while a higher TVaR indicates a larger expected loss once that threshold has been exceeded. Higher TV and TVP values reflect greater variability and uncertainty beyond the selected quantile. The larger values produced by the TL-MK-LLoGP distribution therefore indicate a more conservative assessment of extreme-loss exposure under the parameter settings considered. However, heavier tails do not automatically imply that a model is better. Their suitability depends on whether the observed data support substantial tail risk and should be assessed together with goodness-of-fit measures and the application context.

Table 9.1. Estimated Risk Measures for Selected Distributions at Specified Confidence Levels and Parameter Values

Distribution	**Risk Measure**	**0.70**	**0.75**	**0.80**	**0.85**	**0.90**	**0.95**
TL-MK-LLoGP	VaR	0.1463	0.2399	0.4000	0.6945	1.3143	3.0791
(α=1.12, β=1.3, θ=0.8, c=0.25)	TVaR	1.9462	2.2948	2.7889	3.5467	4.8766	7.9883
	TV	29.3216	34.4569	41.8507	53.4986	74.8956	129.7843
	TVP	22.4713	28.1375	36.2694	49.0205	72.2827	131.2833
TL-MK-LLoGP	VaR	0.1117	0.1887	0.3238	0.5784	0.1273	2.7320
(α=1, β=1.3, θ=0.8, c=0.25)	TVaR	1.7537	2.0730	2.5276	3.2289	4.4680	7.3937
	TV	26.4944	31.1819	37.9441	48.6211	68.2911	118.9585
	TVP	20.2998	25.4594	32.8828	44.5569	65.9300	120.4043
APW	VaR	0.1283	0.1540	0.1871	0.2322	0.3001	0.4273
(α=1.958, β=0.7, λ=0.6)	TVaR	0.2970	0.3282	0.3679	0.4210	0.4998	0.6443
	TV	0.0410	0.0431	0.0458	0.0492	0.0541	0.0628
	TVP	0.3257	0.3606	0.4045	0.4628	0.5485	0.7040
APTLW	VaR	0.0020	0.0046	0.0107	0.0245	0.0564	0.1424
(α=1.8, β=0.2, c=0.5, λ=0.05)	TVaR	0.6531	0.7305	0.8341	0.9842	1.2350	1.8008
	TV	0.1634	0.1849	0.2056	0.2313	0.2642	0.2706
	TVP	0.7674	0.8692	0.9986	1.1808	1.4728	2.0579

10. Applications

The usefulness of the TL-MK-LLoGP distribution in practical scenarios is highlighted in this section. To evaluate the performance of the TL-MK-LLoGP distribution in comparison with alternative models, several goodness-of-fit statistics are used, including -2 log-likelihood (-2ln(L)), Akaike information criterion (AIC), Corrected

Akaike information criterion (AICc), and Bayesian information criterion (BIC). The analysis further incorporates the Cramér–von Mises (W^*), Anderson–Darling (A^*), and Kolmogorov–Smirnov (K-S) goodness-of-fit statistics along with the associated K-S p-value. Generally, models with smaller values of these statistics and the highest p-value for the K-S statistic are considered to offer a better fit. Moreover, the evaluation includes various graphical tools, such as the total time on test (TTT) scaled plot, Kaplan-Meier (K-M) survival curve, empirical cumulative distribution function (ECDF), profile log-likelihood plots, probability plots, density plots, and the hazard rate function (HRF) plot. Besides the visual interpretation enabled by probability plots, the corresponding sums of squares (SS) from the probability plots and given in Equation (10.1) are calculated. A smaller SS value indicates a better fit to the observed data. These measures of closeness are given by

$$SS = \sum_{j=1}^{n} \left[F_{TL-MK-GPS}(x_{(j)}; \hat{\alpha}, \hat{\beta}, \hat{\theta}, \hat{\psi}) - \left(\frac{j - 0.375}{n + 0.25} \right) \right]^2, \tag{10.1}$$

for each of the fitted distribution, where $x_{(j)}$ is the ordered values of the observed data.

The goodness-of-fit results provide relative comparisons among the fitted candidate models rather than evidence of universal superiority. Where the differences in AIC, BIC, K-S, or related measures are small, the models may have comparable empirical support. Therefore, the results are interpreted as showing that the TL-MK-LLoGP model is competitive and, for the datasets considered, records the most favourable overall fit statistics among the selected models.

The empirical assessment uses three real datasets with different sample sizes and hazard-rate characteristics. The first contains survival times, measured in days, for 73 patients diagnosed with acute bone cancer (Alsaggaf (2024)). The second comprises 46 repair times, measured in hours, for an airborne communication transceiver (Gwazane (2022)). The third contains waiting times, measured in minutes, for 100 bank customers (Alotaibi et al. (2022)). These datasets were selected to examine the performance of the proposed model for medical survival, engineering reliability, and service-time data.

The TL-MK-LLoGP distribution is compared with five flexible four-parameter models: the Topp-Leone Weibull Poisson (TL-WP) distribution (Makubate et al. (2021)), the Topp-Leone type I heavy-tailed log-logistic Poisson (TL-TIHT-LLoGP) distribution (Nkomo et al. (2024)), the odd power generalized Weibull log-logistic Poisson (OP-GW-LLoGP) distribution (Oluyede et al. (2022)), the odd log-logistic logarithmic Weibull (OLLoG-WL) distribution (Alizadeh et al. (2017)), and the Ristić-Balakrishnan heavy-tailed type II Topp-Leone log-logistic (RBHTTIITL-LLoG) distribution (Warahena-Liyanage et al. (2025)). These models provide comparisons with Topp-Leone, Weibull-based, log-logistic, power-series, and heavy-tailed constructions while maintaining the same number of estimated parameters as the proposed model. Consequently, the empirical comparison focuses on fully specified flexible models that are directly estimable for the three datasets. **The PDFs of the competing distributions and the datasets used in this section are provided in the appendix.**

10.1. Survival Times in Acute Bone Cancer

The first real dataset concerns the survival times, measured in days, of 73 patients diagnosed with acute bone cancer and was previously analyzed by Alsaggaf (2024).

The estimated variance-covariance matrix for the TL-MK-LLoGP model on the survival times data set is given by

$$\begin{pmatrix} 6.784 & -9.443 \times 10^{-3} & 3.720 & -0.060 \\ -9.443 \times 10^{-3} & 2.541 \times 10^{-5} & -6.762 \times 10^{-3} & 1.625 \times 10^{-4} \\ 3.720 & -6.762 \times 10^{-3} & 2.609 & -0.043 \\ -0.060 & 1.625 \times 10^{-4} & -0.043 & 0.001 \end{pmatrix},$$

and the 95% confidence intervals for the model parameters are given by
$\alpha \in [17.665 \pm 5.105]$, $\beta \in [1.343 \pm 0.010]$, $\theta \in [4.546 \pm 3.166]$ and $c \in [0.210 \pm 0.063]$, respectively.

Table 10.1 displays the maximum likelihood estimates (MLEs), with standard errors (SEs) shown in parentheses, along with the goodness-of-fit statistics for the survival times in acute bone cancer data. From the values reported in

Table 10.1, it can be concluded that the TL-MK-LLoGP distribution provides a better fit than the competing models, as it yields the smallest values for the goodness-of-fit statistics, including $-2\log(L)$, AIC, AICc, BIC, W^*, A^*, and K-S. Furthermore, among all the distributions evaluated, the TL-MK-LLoGP distribution achieves the highest p-value for the K-S test. The SS value obtained from the probability plot of the TL-MK-LLoGP distribution is also the lowest, further confirming its superior fit relative to the other models.

Table 10.1. **Estimates of Models and Goodness-of-fit Statistics for Survival Times for Acute Bone Cancer Data**

Model	Estimates				Statistics								
	α	β	θ	c	$-2\log(L)$	AIC	$AICc$	BIC	W^*	A^*	$K-S$	P-value	SS
TL-MK-LLoGP	17.665	1.343	4.546	0.210	280.207	288.207	288.795	297.368	0.077	0.593	0.074	0.818	0.058
	(2.605)	(0.005)	(1.615)	(0.032)									
	α	β	b	θ									
TL-WP	2.145	2.337×10^{-01}	$8.345\times10^{+01}$	4.328×10^{-08}	286.080	294.080	294.669	303.242	0.143	1.027	0.093	0.558	0.134
	(5.987×10^{-02})	(1.922×10^{-02})	(3.651×10^{-04})	(1.873×10^{-02})									
	α	β	λ	θ									
OP-GW-LLoGP	3.523	0.030	0.603	7.002	287.713	295.713	296.301	304.875	0.169	1.148	0.117	0.267	0.189
	(0.896)	(0.010)	(0.075)	(2.138)									
	b	λ	δ	β									
TL-TIHT-LLoGP	$1.015\times10^{+02}$	8.558×10^{-03}	5.775×10^{-02}	1.232	289.795	297.795	298.384	306.9557	0.154	1.104	0.115	0.290	0.170
	(1.010×10^{-04})	(2.943×10^{-03})	(4.282×10^{-02})	(2.012×10^{-01})									
	α	β	a	b									
OLLoG-WL	1.069	$1.030\times10^{+02}$	1.614	9.643×10^{-02}	281.890	289.890	290.478	299.052	0.082	0.631	0.010	0.484	0.112
	(3.485×10^{-01})	(2.280×10^{-05})	(2.420×10^{-01})	(2.952×10^{-02})									
	δ	b	θ	c									
RBHTTIITL-LLoG	2.378×10^{-01}	6.113×10^{-04}	$1.084\times10^{+02}$	1.042	282.085	290.085	290.673	299.257	0.085	0.634	0.100	0.453	0.143
	(1.238×10^{-01})	(3.129×10^{-04})	(1.415×10^{-04})	(1.235×10^{-01})									

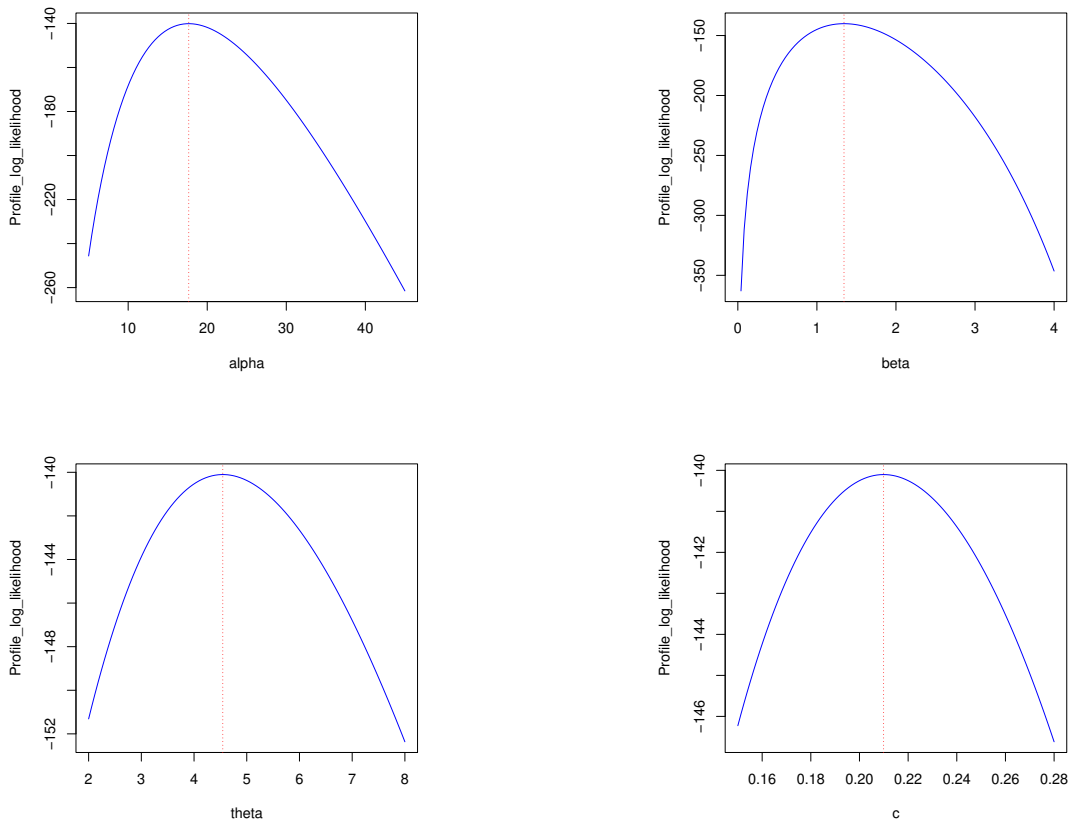


Figure 10.1. Profile Log-Lieklihood Plots for Survival Times for Acute Bone Cancer Data

Figure 10.1 presents the profile log-likelihood plots for the parameters of the TL-MK-LLoGP distribution applied to the survival times of acute cancer data. The plots indicate that the maximum likelihood estimates (MLEs) are unique, demonstrating the identifiability of the parameters of the TL-MK-LLoGP distribution on the acute bone cancer data.

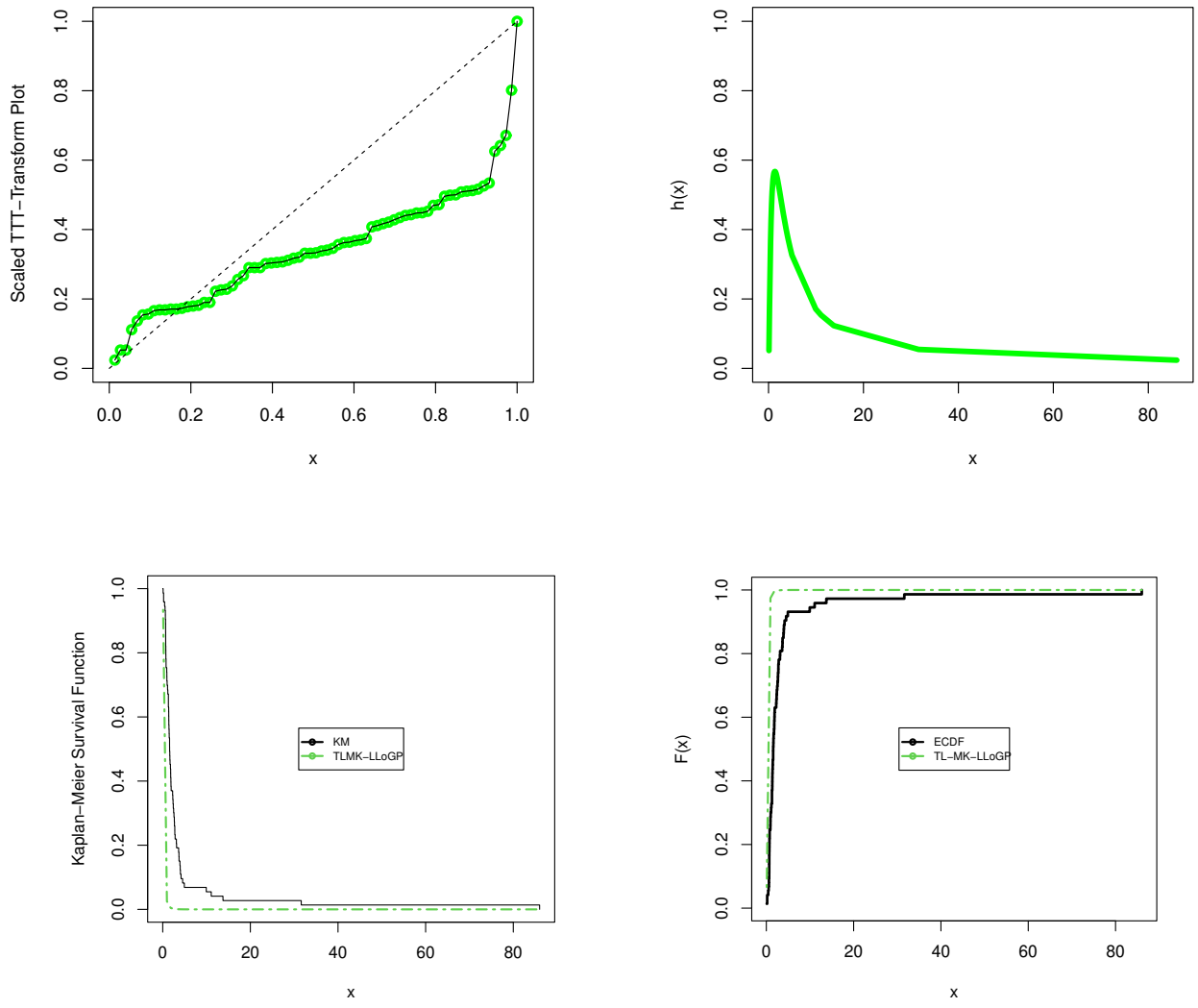


Figure 10.2. Scaled TTT, HRF, K-M Survival and ECDF Plots for TL-MK-LLoGP Survival Times in Acute Bone Cancer Data

Figure 10.2 displays the scaled TTT plot, hazard rate function (HRF), empirical cumulative distribution function (ECDF), and Kaplan–Meier (K-M) survival curves for the bone cancer dataset. The scaled TTT plot suggests an increasing followed by decreasing HRF, which is consistent with the behavior of the HRF plot for TL-MK-LLoGP distribution. Furthermore, the TL-MK-LLoGP distribution closely aligns with both the ECDF and K-M survival curves, indicating a good fit for the observed survival times from the acute bone cancer data.

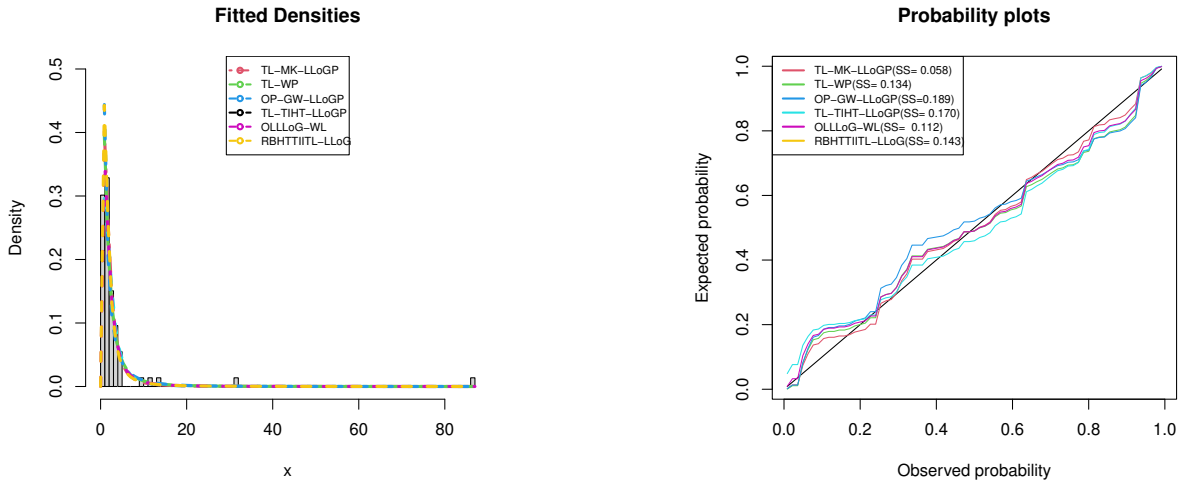


Figure 10.3. Fitted Densities and Probability Plots for Survival Times in Acute Bone Cancer Data

Figure 10.3 agrees with the results presented in Table 10.1. These plots show that the TL-MK-LLoGP captures the survival-time data better than other fitted distributions, as it has the least sum of squares value.

10.2. Repair Lifetimes of an Airborne Transceiver

These data correspond to the maintenance of active repair times (in hours) for an airborne communication transceiver of size n = 46. The data were recently analyzed by Gwazane (2022).

The estimated variance-covariance matrix for the TL-MK-LLoGP model on the repair lifetimes data set is given by

$$\begin{pmatrix} 5.316\times10^{-18} & -2.892\times10^{-18} & -3.093\times10^{-17} & -3.174\times10^{-13} \\ -2.892\times10^{-18} & 1.573\times10^{-18} & 1.682\times10^{-17} & 1.726\times10^{-13} \\ -3.092\times10^{-17} & 1.682\times10^{-17} & 1.798\times10^{-16} & 1.846\times10^{-12} \\ -3.174\times10^{-13} & 1.726\times10^{-13} & 1.846\times10^{-12} & 1.895 \end{pmatrix},$$

and the 95% confidence intervals for the model parameters are given by $\alpha \in [2.128\times10^{+01} \pm 4.519\times10^{-09}]$, $\beta \in [1.449\times10^{+02} \pm 2.458\times10^{-09}]$, $\theta \in [7.092 \pm 2.629\times10^{-08}]$ and $c \in [1.324\times10^{-03} \pm 2.698\times10^{-04}]$, respectively.

Table 10.2. **Estimates of Models and Goodness-of-fit Statistics for Repair Lifetimes of an Airborne Transceiver Data**

Model	Estimates				Statistics								
	α	β	θ	c	$-2\log(L)$	AIC	$AICc$	BIC	W^*	A^*	$K-S$	P-value	SS
TL-MK-LLoGP	$2.128\times10^{+01}$	$1.449\times10^{+02}$	7.092	1.324×10^{-03}	201.385	209.385	210.361	216.700	0.065	0.399	0.095	0.805	0.059
	(2.306×10^{-09})	(1.254×10^{-09})	(1.341×10^{-08})	(1.376×10^{-04})									
	α	β	b	θ									
TL-WP	1.932×10^{-01}	8.583×10^{-01}	1.128	1.279×10^{-08}	208.09	216.059	217.034	223.373	0.123	0.852	0.123	0.492	0.114
	(5.987×10^{-02})	(1.922×10^{-02})	(3.651×10^{-04})	(1.873×10^{-02})									
	α	β	λ	θ									
OP-GW-LLoGP	$2.184\times10^{+01}$	9.009×10^{-04}	3.061×10^{-01}	$5.463\times10^{+01}$	211.463	219.463	220.439	226.7785	0.088	0.718	0.167	0.155	0.350
	(1.261×10^{-04})	(1.434×10^{-04})	(3.466×10^{-02})	(5.267×10^{-08})									
	b	λ	δ	β									
TL-TIHT-LLoGP	19.722$\times10^{+01}$	7.393×10^{-03}	4.497×10^{-02}	1.174	208.025	216.025	217.000	223.339	0.117	0.727	0.103	0.709	0.077
	(2.342×10^{-04})	(5.499×10^{-03})	(7.524×10^{-02})	(3.957×10^{-01})									
	α	β	a	b									
OLLoG-WL	1.851	$1.033\times10^{+02}$	1.230	8.707×10^{-02}	203.581	211.581	212.557	218.896	0.083	0.524	0.098	0.772	0.060
	(2.048)	(3.956×10^{-03})	(3.605×10^{-01})	(4.767×10^{-02})									
	δ	b	θ	c									
RNHTTIITL-LLoG	$1.452\times10^{+01}$	1.320×10^{-04}	1.117×10^{-01}	3.724	232.088	240.088	241.064	247.403	0.342	2.015	0.192	0.067	0.487
	(5.547×10^{-03})	(3.212×10^{-04})	(1.373×10^{-01})	(7.628×10^{-04})									

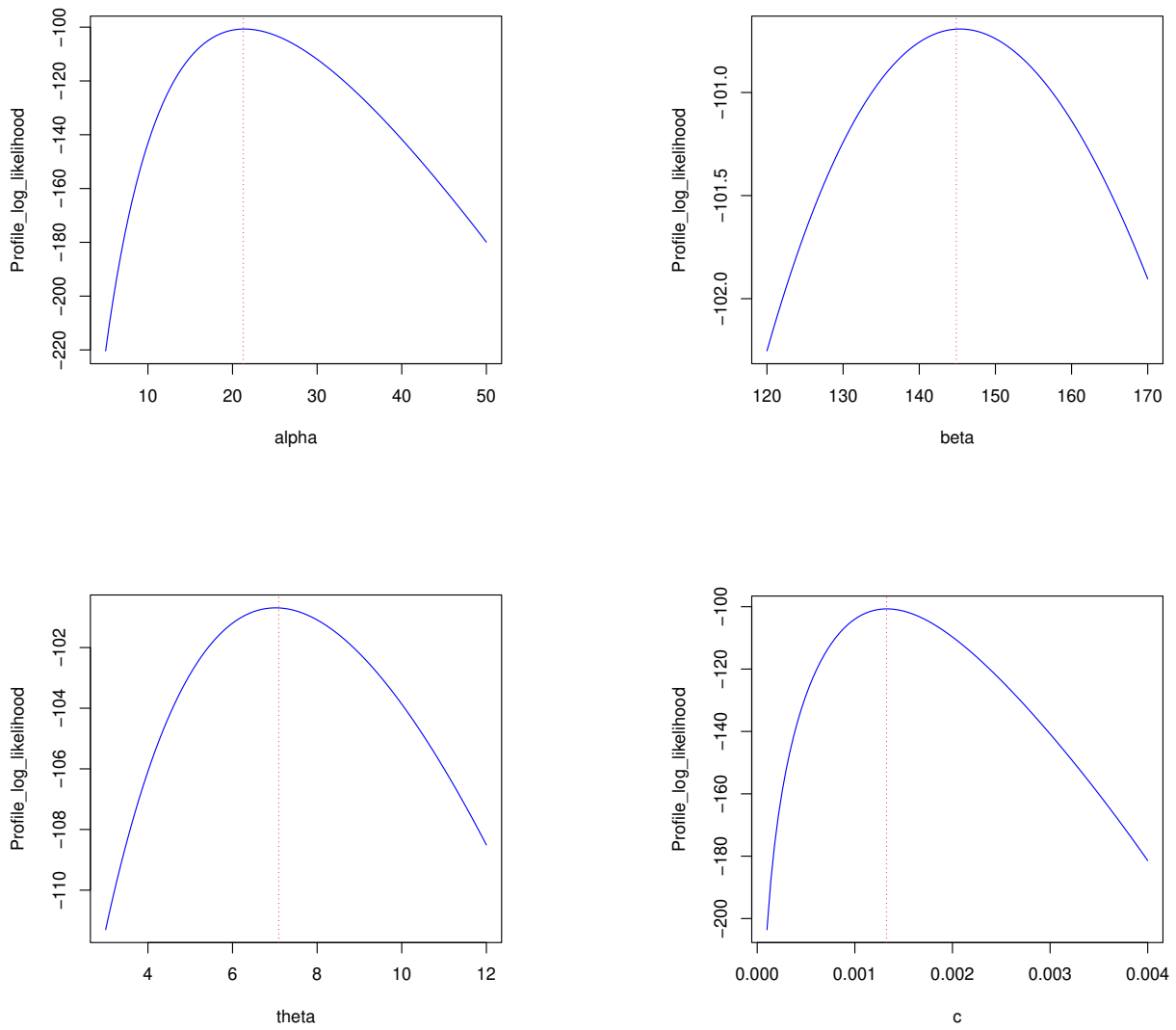


Figure 10.4. Profile Log-Likelihood Plots for Repair Lifetimes of an Airborne Transceiver Data

Figure 10.4 displays the profile log-likelihood plots for the parameters of the TL-MK-LLoGP distribution based on the repair lifetime data. The uniqueness of the MLEs evident in the graphs confirms the identifiability of the parameters of the TL-MK-LLoGP distribution on the repair lifetimes of an airbone transceiver data.

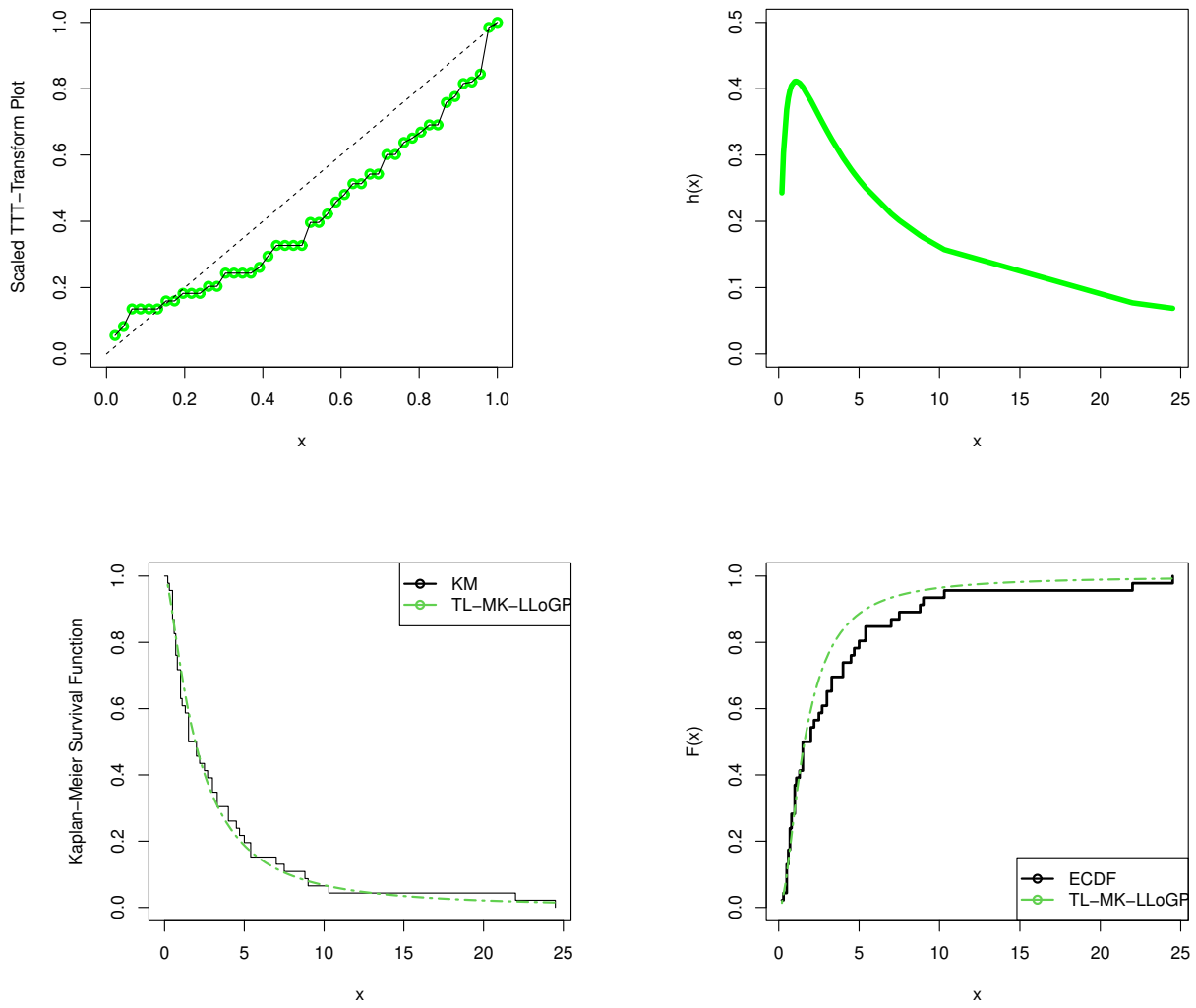


Figure 10.5. Scaled TTT, HRF, K-M Survival and ECDF Plots for TL-MK-LLoGP Repair Times for an Airborne Communication Transceive Data

Figure 10.5 illustrates the scaled TTT plot, HRF, ECDF, and K–M survival curves for the repair times of an airborne communication transceiver dataset. The scaled TTT plot reveals an increasing followed by a decreasing failure rate and it is in agreement with the HRF plot, reflecting the characteristic behavior of the TL-MK-LLoGP distribution. In addition, the TL-MK-LLoGP model closely follows both the ECDF and K–M curves, demonstrating a good fit to the observed repair times data.

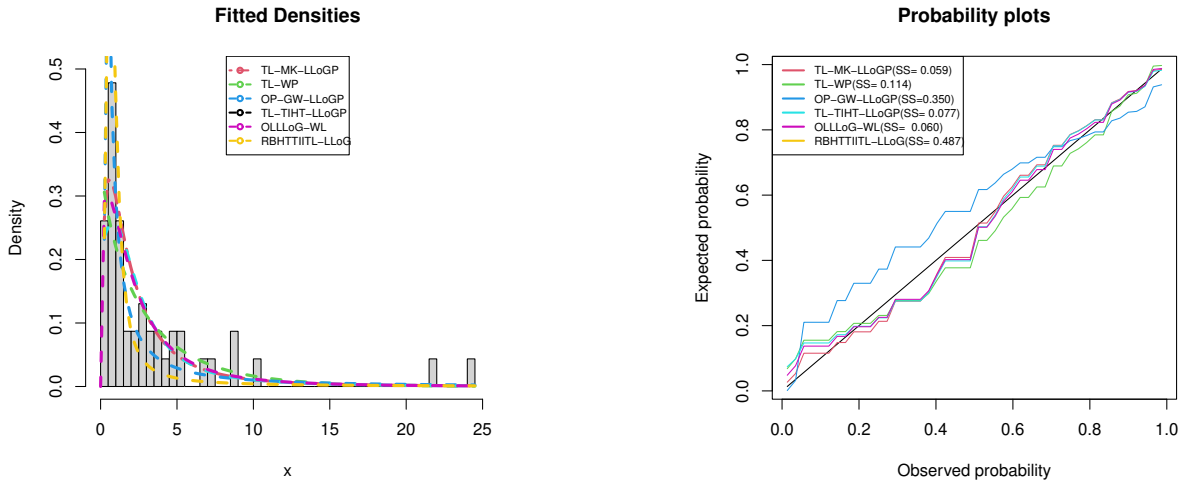


Figure 10.6. Fitted Densities and Probability Plots for Repair Lifetimes Data

Figure 10.6 displays the probability plots for the TL-MK-LLoGP distribution as well as other existing distributions. The TL-MK-LLoGP distribution fit the repair lifetimes data best compared to the other distributions as it presented the lowest sum of squares value.

10.3. Waiting Times of Bank Customers

The data entails waiting times in minutes for 100 bank customers and it was analyzed by Alotaibi et al. (2022).

The estimated variance-covariance matrix for the TL-MK-LLoGP model on the waiting times data set is given by

$$\begin{pmatrix} 8.833 & -6.769\times10^{-06} & -6.163\times10^{-01} & 2.231\times10^{-03} \\ -6.769\times10^{-06} & 5.694\times10^{-12} & 4.723\times10^{-07} & -1.420\times10^{-09} \\ -6.163\times10^{-01} & 4.723\times10^{-07} & 4.300\times10^{-02} & -1.557\times10^{-04} \\ 2.231\times10^{-03} & -1.420\times10^{-09} & -1.557\times10^{-04} & 7.287\times10^{-07} \end{pmatrix},$$

and the 95% confidence intervals for the model parameters are given by $\alpha \in [5.979\times10^{+01} \pm 5.825]$, $\beta \in [8.265 \pm 4.677\times10^{-06}]$, $\theta \in [8.131\times10^{+01} \pm 4.064\times10^{-01}]$ and $c \in [1.145\times10^{-02} \pm 1.673\times10^{-03}]$, respectively.

Table 10.3. **Estimates of Models and Goodness-of-fit Statistics for Waiting Times of Bank Customers Data**

Model	Estimates				Statistics								
	α	β	θ	c	$-2\log(L)$	AIC	$AICc$	BIC	W^*	A^*	$K-S$	P-value	SS
TL-MK-LLoGP	$5.979\times10^{+01}$ (2.972)	8.265 (2.386×10^{-06})	$8.131\times10^{+01}$ (2.074×10^{-01})	1.448×10^{-02} (8.536×10^{-04})	634.066	642.066	642.487	652.486	0.018	0.131	0.037	0.993	0.018
	α	β	b	θ									
TL-WP	7.788×10^{-02} (2.412×10^{-02})	9.010×10^{-01} (9.352×10^{-02})	1.329 (2.144×10^{-01})	7.887×10^{-09} (8.233×10^{-03})	652.540	660.540	660.961	670.960	0.021	0.145	0.155	0.017	0.531
	α	β	λ	θ									
OP-GW-LLoGP	9.907×10^{-01} (3.167×10^{-01})	8.678×10^{-02} (3.109×10^{-02})	8.711×10^{-01} (7.413×10^{-02})	1.130×10^{-08} (7.755×10^{-03})	652.275	660.275	660.696	670.696	0.154	0.963	0.124	0.095	0.300
	b	λ	δ	β									
TL-TIHT-LLoGP	4.382×10^{-08} (1.620×10^{-02})	5.816×10^{-01} (2.350×10^{-01})	1.049×10^{-02} (3.314)	(9.480×10^{-01}) (2.217×10^{-01})	668.286	676.287	676.708	686.707	0.209	1.430	0.160	0.012	0.743
	α	β	a	b									
OLLoGP-WL	234.535 (0.287)	23.809 (2.795)	1.463 (0.110)	52.191 (1.865)	637.3484	645.384	645.805	655.805	0.062	0.391	0.057	0.897	0.058
	δ	b	θ	c									
RBHTTIITL-LLoG	$1.397\times10^{+01}$ (6.413×10^{-11})	1.839 (2.704×10^{-10})	2.661×10^{-05} (4.972×10^{-06})	2.283 (2.472×10^{-10})	655.048	663.047	663.468	673.468	0.055	0.421	0.103	0.243	0.192

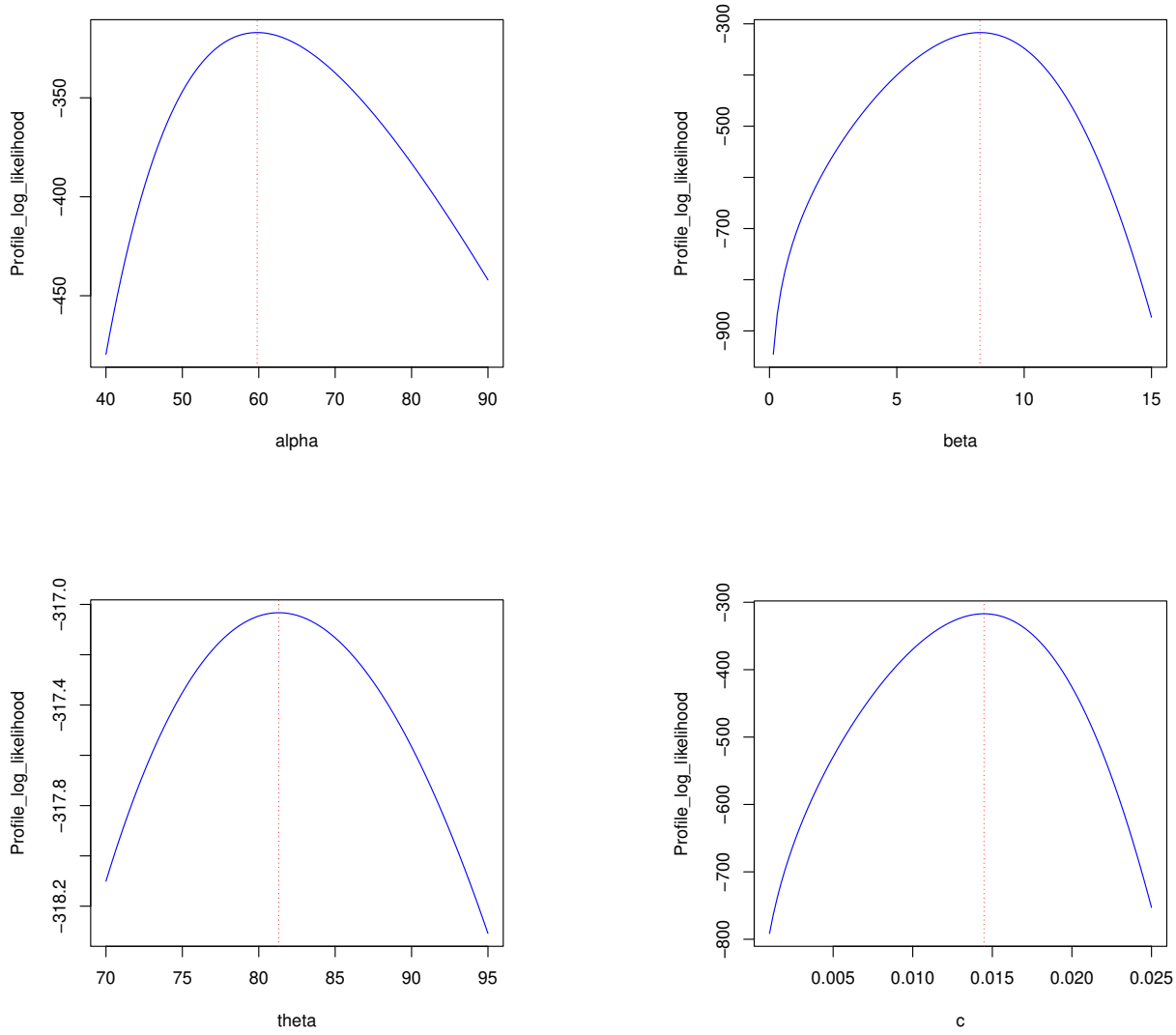


Figure 10.7. Profile Plots for Waiting times of Bank Customers Data

Figure 10.7 shows the profile log-likelihood plots for the parameters of the TL-MK-LLoGP distribution fitted to the waiting time data. The uniqueness of the MLEs confirms the identifiability of the model parameters.

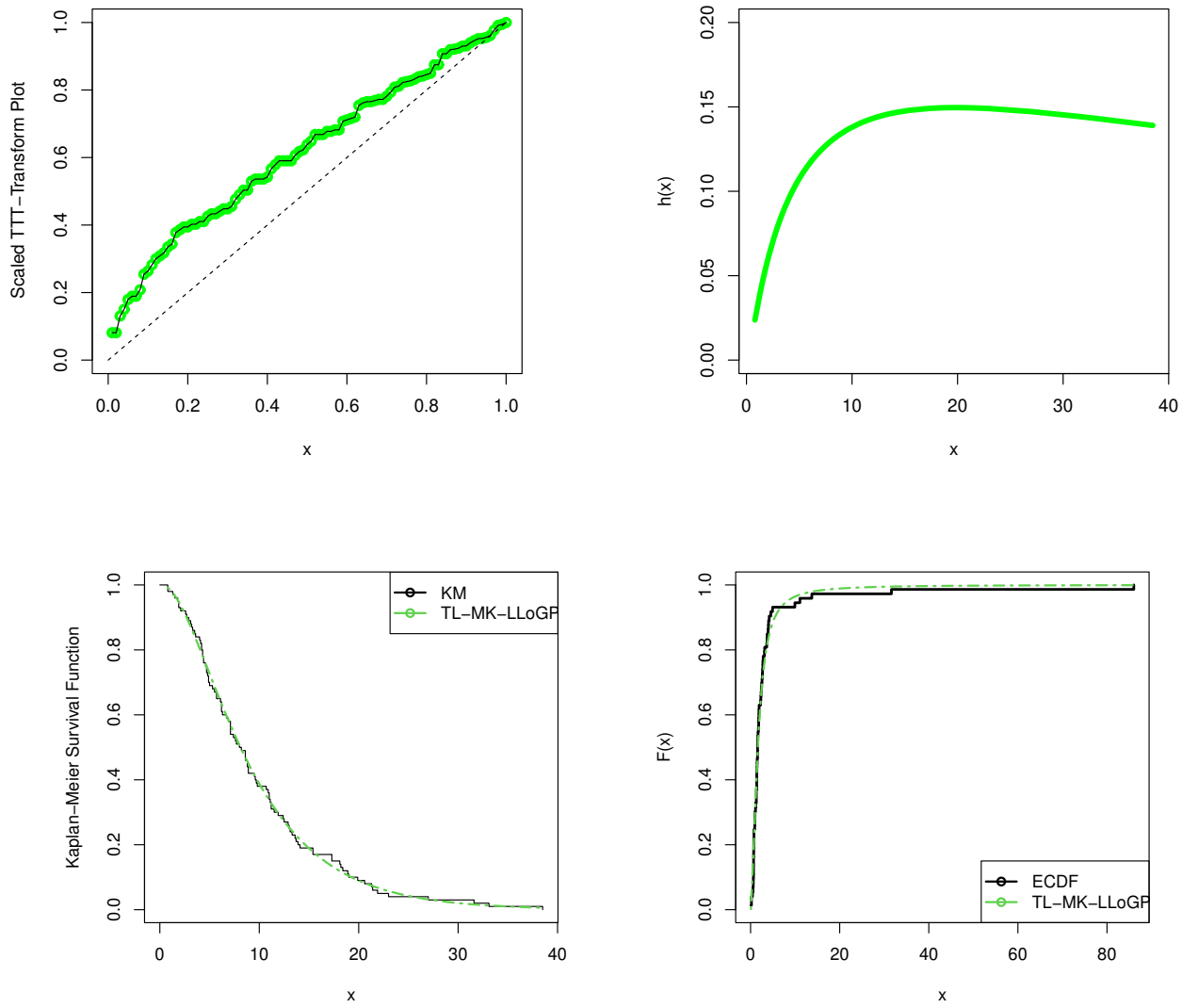


Figure 10.8. Scaled TTT, HRF, K-M Survival and ECDF Plots for TL-MK-LLoGP Waiting Times for Bank Customers Data

Figure 10.8 presents the scaled total scaled TTT plot, HRF, ECDF, and K–M survival curves for the waiting times for customers dataset. The scaled TTT plot indicates an increasing HRF, which aligns with the expected pattern of the TL-MK-LLoGP distribution. Additionally, the TL-MK-LLoGP model shows a strong agreement with both the ECDF and K–M survival curves, suggesting it provides a good fit to the Waiting times for bank customers data.

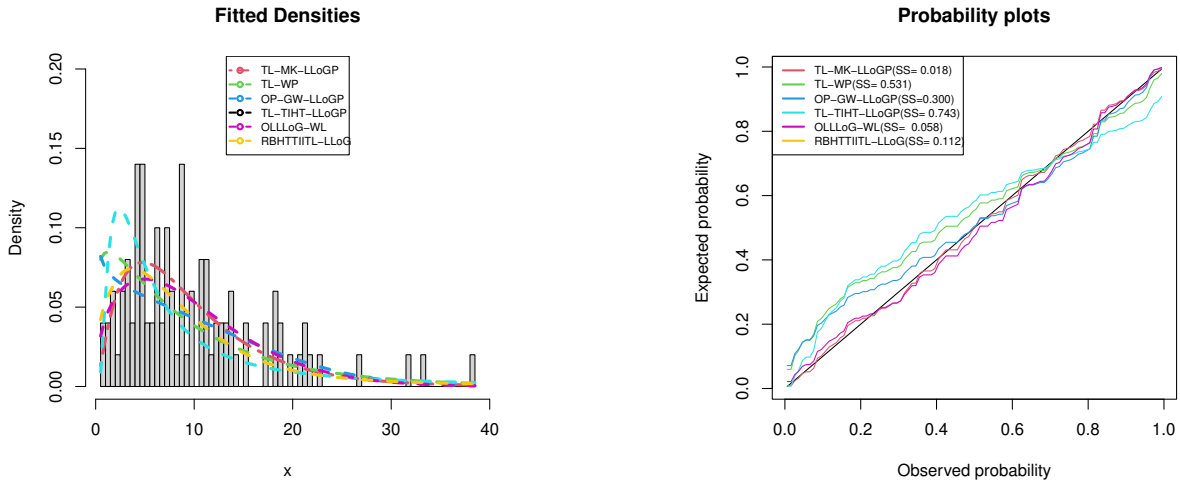


Figure 10.9. Fitted Densities and Probability Plots for Waiting Times Data

Figure 10.9 supports the findings in Table 10.3. The TL-MK-LLoGP distribution provides a competitive fit and records the most favourable overall fit measures among the models fitted to the waiting-time data.

Across the three datasets, the TL-MK-LLoGP distribution produced the smallest reported AIC and BIC values among the fitted models. For the acute bone cancer data, its AIC and BIC values were 288.207 and 297.368, respectively, compared with 289.890 and 299.052 for the nearest competing model. For the airborne-transceiver repair data, the corresponding values were 209.385 and 216.700, compared with 211.581 and 218.896. For the bank waiting-time data, they were 642.066 and 652.486, compared with 645.384 and 655.805. These results indicate better relative fit among the models examined, although the size of the improvement varies across the datasets.

11. Discussion and Limitations

The fitted TL-MK-LLoGP distribution has four free parameters, as in each of the competing model. Its additional transformations provide greater control over density and hazard-rate shapes, but may also increase parameter dependence and sensitivity near boundary values. AIC, AICc, and BIC account for model dimension when comparing fitted models, although these criteria do not eliminate the possibility of overfitting. The profile log-likelihood plots, standard errors, and variance-covariance matrices provide dataset-specific evidence on estimation stability rather than a general guarantee of global identifiability.

The manuscript identifies submodels obtained by removing the power-series component or fixing selected shape parameters. However, these nested submodels were not fitted separately to determine whether they perform nearly as well as the complete TL-MK-LLoGP model. The reported fit advantages should therefore be interpreted relative to the competing models examined, rather than as evidence that every component is necessary for every dataset. Direct comparison with the nested submodels remains an area for further study.

For the fitted special cases, the power-series normalizing functions are available in closed form, and one objective-function evaluation remains of order $O(n)$. The nested transformations and four-dimensional optimization may nevertheless require more computation than simpler models. Direct execution times were not recorded, so the study does not claim that the proposed model is computationally faster than its alternatives.

The simulation analysis is not restricted to the TL-MK-LLoGP special case, as additional simulation studies for other TL-MK-GPS special cases (TL-MK-LinLog and TL-MK-UG) are reported in the appendix. The reported simulation results remain conditional on successful numerical convergence. Furthermore, the three applications assess in-sample fit and do not include cross-validation. Therefore, although the findings provide evidence supporting the proposed model and the special cases examined, they should not be interpreted as establishing superiority across all TL-MK-GPS submodels or datasets.

12. Conclusion

In this study, we introduced the Topp-Leone modified Kies-G power series (TL-MK-GPS) distribution, a flexible class of distributions designed to model data with complex hazard rate behaviors. The distribution's PDF, CDF, and HRF were derived and discussed. Additionally, various properties were derived. Numerical analyses highlighted the distribution's effectiveness in capturing diverse data characteristics. Five estimation methods were examined, with maximum likelihood providing the most favourable performance under the simulation settings considered. The versatility of the TL-MK-GPS class of distributions was further illustrated through its application to real-world datasets. We recommend future research to explore bivariate extensions and Bayesian estimation techniques to enhance the utility and applicability of this distribution in broader contexts.

Appendix

Click on the link below for results in the appendix.
https://drive.google.com/file/d/1Scjnhpb5nl6uOAvBzxYuczJJMDKyLC3o/view?usp=sharing

REFERENCES

Al-Babtain, A. A., Shakhatreh, M. K., Nassar, M., and Afify, A. Z., 2020. *A New Modified Kies Family: Properties, Estimation Under Complete and Type-II Censored Samples, and Engineering Applications,* Mathematics, 8(8), 13-45.

Al-Shomrani, A., Arif, O., Shawky, A., Hanif, S., and Shahbaz, M. Q., 2016. *Topp-Leone Family of Distributions: Some Properties and Application,* Pakistan Journal of Statistics and Operation Research, 12(3), 443–451.

Alizadeh, M., Cordeiro, G. M., Brito, E. d., and Demeétrio, C. G., 2015. *The Beta Marshall-Olkin Family of Distributions,* Journal of Statistical Distributions and Applications, 2, 1–18.

Alizadeh, M., MirMostafee, S. M. T. K., Ortega, E. M. M., Ramires, T. G., and Cordeiro, G. M., 2017. *The Odd Log-Logistic Logarithmic Generated Family of Distributions with Applications in Different Areas,* Journal of Statistical Distributions and Applications, 4(1), 6.

Al Mutairi, A., Iqbal, M. Z., Arshad, M. Z., Alnssyan, B., Al-Mofleh, H., and Afify, A. Z. (2021). *A New Extended Model with Bathtub-shaped Failure Rate: Properties, Inference, Simulation, and Applications*. Mathematics, 9(17), Article 2024. doi.org/10.3390/math9172024

Alsaggaf, I., 2024. *Analyzing Cancer Survival Times Using the Exponentiated Fréchet-Gompertz Distribution,* European Journal of Pure and Applied Mathematics, 17(4), 3856–3898.

Alzaatreh, A., Lee, C., and Famoye, F., 2013. *A New Method for Generating Families of Continuous Distributions,* Metron, 71(1), 63–79.

Benkhelifa, L., 2022. *Alpha Power Topp-Leone Weibull Distribution: Properties, Characterizations, Regression Modelling and Applications,* Journal of Statistics and Management Systems, 25(8), 1945–1970.

Bourguignon, M., Silva, R. B., and Cordeiro, G. M., 2014. *The Weibull-G Family of Probability Distributions,* Journal of Data Science, 12(1), 53–68.

Chamunorwa, S., Oluyede, B., Moakofi, T., and Chipepa, F., 2024. *The Type II Exponentiated Half Logistic-Gompertz-G Power Series Class of Distributions: Properties and Applications,* Statistics, Optimization & Information Computing, 12(2), 381–399. doi:10.19139/soic-2310-5070-1721.

Chipepa, F., Oluyede, B., and Makubate, B., 2020. *The Topp-Leone-Marshall-Olkin-G family of Distributions with Applications,* International Journal of Statistics and Probability, 9(4), 15–32.

Gabanakgosi, M., and Oluyede, B., 2024. *The Topp-Leone-Gompertz-G Power Series Class of Distributions with Applications,* Pakistan Journal of Statistics and Operation Research, 20(2), 171–195. doi:10.18187/pjsor.v20i2.4032.

Glaser, R. E. (1980). *Bathtub and Related Failure Rate Characterizations*. Journal of the American Statistical Association, 75(371), 667–672. doi.org/10.1080/01621459.1980.10477530

Gwazane, M., 2022. *On Some Exponentiated Generalised Families and Compound Class of Distributions With Applications (Master's Thesis),* Botswana International University of Science and Technology (Botswana).

Hassan, A., Rashid, A., and Akhtar, N., 2020. *Exponentiated Quasi Power Lindley Power Series Distribution with Applications in Medical Science,* Journal of Applied Mathematics, Statistics and Informatics, 16(1), 37–60.

Makubate, B., Moakofi, T., and Oluyede, B., 2021. *A New Generalized Lindley-Weibull Class of Distributions: Theory, Properties and Applications,* Mathematica Slovaca, 71(1), 211–234.

Makubate, B., Rannona, K., Oluyede, B., and Chipepa, F., 2021. *The Topp-Leone-G Power Series Class of Distributions with Applications,* Pakistan Journal of Statistics and Operation Research, 17, 827–846.

Moakofi, T., Oluyede, B., and Gabanakgosi, M., 2022. *The Topp-Leone Odd Burr III-G Family of Distributions: Model, Properties and Applications,* Statistics, Optimization & Information Computing, 10(1), 236–262. doi:10.19139/soic-2310-5070-1135.

Alotaibi, N., Elbatal, I., Almetwally, E. M., Alyami, S. A., Al-Moisheer, A. S., and Elgarhy, M., 2022. *Bivariate Step-Stress Accelerated Life Tests for the Kavya–Manoharan Exponentiated Weibull Model under Progressive Censoring with Applications,* Symmetry, 14(9), 1791.

Nassar, M., Alzaatreh, A., Mead, M., and Abo-Kasem, O., 2017. *Alpha Power Weibull Distribution: Properties and Applications,* Communications in Statistics — Theory and Methods, 46(20), 10236–10252.

Nkomo, W., Oluyede, B., and Chipepa, F., 2024. *Topp-Leone Type I Heavy-Tailed-G Power Series Class of Distributions: Properties, Risk Measures, and Applications,* Statistics, Optimization & Information Computing, 13(1), 88–110. doi:10.19139/soic-2310-5070-2039.

Oluyede, B., and Chipepa, F., 2023. *The Marshall-Olkin Odd Exponential Half Logistic-G Family of Distributions: Properties and Applications,* Statistics, Optimization & Information Computing, 11(2), 479–503.

Oluyede, B., Dingalo, N., and Chipepa, F., 2023. *The Topp-Leone-Harris-G Family of Distributions with Applications,* International Journal of Mathematics in Operational Research, 24(4), 554–582.

Oluyede, B., Gabanakgosi, M., and Warahena-Liyanage, G., 2024. *The Marshall-Olkin-Topp-Leone-Gompertz-G Family of Distributions with Applications,* Statistics, Optimization & Information Computing, 12(4), 882–906. doi:10.19139/soic-2310-5070-1509.

Oluyede, B. O., Mashabe, B., Fagbamigbe, A., Makubate, B., and Wanduku, D., 2020. *The Exponentiated Generalized Power Series: Family of Distributions: Theory, Properties and Applications,* Heliyon, 6(8), e04653.

Oluyede, B., Moakofi, T., and Chipepa, F., 2022. *The Odd Power Generalized Weibull-G Power Series Class of Distributions: Properties and Applications,* Statistics in Transition (new series), 23(1), 89–108.

Oluyede, B., Moakofi, T., and Lekono, G., 2025. *The New Marshall-Olkin Type II Exponentiated Half-Logistic Odd Burr X-G Family of Distributions with Properties and Applications,* Stats, 8(2), 26.

Oluyede, B., Pu, S., Makubate, B., and Qiu, Y., 2018. *The Gamma-Weibull-G Family of Distributions with Applications,* Austrian Journal of Statistics, 47(1), 45–76.

Oluyede, B., Tlhaloganyang, B. P., and Sengweni, W., 2023. *The Topp-Leone Odd Burr X-G Family of Distributions: Properties and Applications,* Statistics, Optimization & Information Computing, 12(1), 109–132. doi:10.19139/soic-2310-5070-1673.

Osatohanmwen, P., Oyegue, F. O., and Ogbonmwan, S. M. (2020). *The T–R* $\{Y\}$ *Power Series Family of Probability Distributions*. Journal of the Egyptian Mathematical Society, 28(29). doi.org/10.1186/s42787-020-00083-7

Rannona, K., Oluyede, B., Chipepa, F., and Makubate, B., 2022. *The Marshall-Olkin Exponentiated Odd Exponential Half-Logistic-G Family of Distributions with Applications,* Eurasian Bulletin of Mathematics, 4(3), 134–161.

Silva, R., and Cordeiro, G., 2013. *The Burr XII Power Series Distributions: A New Compounding Family,* Brazilian Journal of Probability and Statistics, 29. doi:10.1214/13-BJPS234.

Swetha, P. S. S., and Nagarjuna, V. B., 2025. *Topp-Leone Modified Kies-G Family of Distributions: Properties, Actuarial Measures, Inference and Applications,* Computational Journal of Mathematical and Statistical Sciences, 4(2), 697–737. doi:10.21608/cjmss.2025.418412.1253.

Tahir, M. H., Zubair, M., Mansoor, M., Cordeiro, G. M., Alizadehk, M., and Hamedani, G. G., 2016. *A New Weibull-G Family of Distributions,* Hacettepe Journal of Mathematics and Statistics, 45(2), 629–647.

Tlhaloganyang, B. P., Sengweni, W., and Oluyede, B., 2022. *The Gamma Odd Burr X-G Family of Distributions with Applications,* Pakistan Journal of Statistics and Operation Research, 18, 721–746.

Warahena-Liyanage, G., Oluyede, B., and Moakofi, T., 2025. *The New Ristić-Balakrishnan-Heavy-Tailed-Type II Topp-Leone-G Family of Distributions with Applications,* Journal of Statistical Theory and Applications, 24, 1–40.